7-1-2020

Multidimensional molecular high-harmonic spectroscopy: A road map for charge migration studies

Daniel R. Tuthill
The Ohio State University

François Mauger
Louisiana State University

Timothy D. Scarborough
The Ohio State University

Robert R. Jones
University of Virginia

Mette B. Gaarde
Louisiana State University

See next page for additional authors

Recommended Citation

Tuthill, D., Mauger, F., Scarborough, T., Jones, R., Gaarde, M., Lopata, K., Schafer, K., & DiMauro, L. (2020). Multidimensional molecular high-harmonic spectroscopy: A road map for charge migration studies. *Journal of Molecular Spectroscopy, 372* https://doi.org/10.1016/j.jms.2020.111353

Version of Record: https://www.sciencedirect.com/science/article/pii/S0022285220301211
Manuscript_39316282abc9d891b6b920208f778faa

Multidimensional molecular high-harmonic spectroscopy: a road map for charge migration studies

Daniel R. Tuthill[a,*], François Mauger[b], Timothy D. Scarborough[a], Robert R. Jones[c], Mette B. Gaarde[b], Kenneth Lopata[d], Kenneth J. Schafer[b] and Louis F. DiMauro[a]

[a]Department of Physics, The Ohio State University, Columbus, Ohio 43210, USA
[b]Department of Physics and Astronomy, Louisiana State University, Baton Rouge, Louisiana 70803-4001, USA
[c]Department of Physics, University of Virginia, Charlottesville, Virginia 22904-4714, USA
[d]Department of Chemistry, Louisiana State University, Baton Rouge, Louisiana 70803-4001, USA

ARTICLE INFO

Keywords:
High-harmonic spectroscopy
Charge migration
Two-center interference
Cooper minimum
HHG short trajectory selection

ABSTRACT

This review discusses recent experimental and theoretical analyses of high-harmonic spectroscopy in small molecules, with the aim of characterizing charge migration. We discuss the formulation of molecular high-harmonic spectra followed by methods to extract molecular-target-specific information, both in experiments and ab-initio simulations. We present measured and simulated high-harmonic spectra from carbon dioxide and carbonyl sulfide to illustrate the necessity for multidimensional analyses for high-harmonic spectroscopies that include both the spectral amplitude and phase. Leveraging these results, we examine how such multidimensional analyses pave the way for the study of charge migration with high-harmonic spectroscopy and illustrate the beneficial role a static molecular feature can play when probing dynamics. Finally, we briefly expand our scope with an outlook on the critical role of integrating theoretical and experimental approaches, beyond just high-harmonic spectroscopy, for the development of versatile harmonic spectroscopic probes of charge migration.

1. Introduction

Rapid redistribution of charge following molecular ionization can begin in less than a femtosecond. This response can manifest as an oscillation of the charge throughout the molecule, known as charge migration [1]. Charge migration is predominately due to electron correlation, with a possible weak coupling to nuclear dynamics and the external system, and therefore offers a direct pathway towards studying electron correlation [2, 3]. It has been proposed that these migrations have a significant impact on subsequent charge transfer [4] and bond rearrangement processes [5]. Characterization of charge migration would hence offer insight into possible molecular relaxation pathways [6], and coherent control of the migration could translate to chemical reactions [7].

Measuring charge migration is a formidable challenge because it requires ultrafine spatial (angstrom) and ultrafast temporal (attosecond) resolution probes. The challenge is to unequivocally connect specific charge migration dynamics to the signals being recorded. Beyond case-by-case analyses, it therefore requires concerted experimental and theoretical efforts. Charge migration studies began over two decades ago with early theoretical efforts focused on the underlying mechanism for the migration, and the key aspects of molecules that control it [4, 5, 8, 9, 10]. The simultaneous advancement of attosecond light sources enabled initial studies of static features in atoms [11, 12, 13, 14], such as photoemission delays and hole localization [15, 16, 17]. Within the last decade experimental capabilities entered the attosecond regime [6, 18, 19], leading to the first measurement of charge migration in phenylalanine using molecular fragmentation [20]. Shortly afterwards, high-harmonic spectroscopy was utilized to measure charge migration in iodoacetylene [21] followed by other fragmentation measurements in tryptophan and again phenylalanine [22]. Along the way, charge migration theory has advanced towards a more comprehensive understanding of the migration dynamics, factoring in elements such as nuclear dynamics [23], core-hole excitations [24], and more advanced frameworks for simulations [25]. The potential of core-hole excitations, which are highly localized leading to charge migration in the valence shell, has resulted in new experimental avenues for using free-electron lasers to perform attosecond pump, attosecond probe charge migration studies [26].

In this paper, we review recent efforts towards developing high-harmonic spectroscopy (HHS) as a coherent probe of charge migration. In particular, we review recent experimental and theoretical work using HHS to characterize structural molecular features, and we discuss how such studies provide a roadmap toward HHS-characterization of charge migration without the need for complex reconstruction algorithms. In general, HHS uses the coherence of high-harmonic generation (HHG) [27, 28, 29] as a spectroscopic probe of the emitting molecule's structure. It has been employed to probe static features in molecules such as internuclear distances [30, 31, 32], electronic structure [18, 33, 34, 35, 36], and molecular wave functions [37, 38, 39, 40]. Charge migration studies with HHS hence aim to harness the natural attosecond time scale embedded in the harmonic emission process [41, 42, 43, 44, 45, 46] to extend the probe to molecular dynamics. The natural sub-cycle resolution offered by

*Corresponding Author
tuthill.15@osu.edu (D.R. Tuthill)
ORCID(s): 0000-0002-8101-0635 (D.R. Tuthill); 0000-0001-7555-6001 (F. Mauger); 0000-0001-9382-1323 (T.D. Scarborough); 0000-0001-5808-6781 (R.R. Jones); 0000-0002-9141-684X (K. Lopata)

HHS differs from molecular fragmentation, which requires the migration to imprint itself upon the longer fragmentation signals [22]. Thinking of charge migration as a transient redistribution of charge between different regions of a molecule, we suggest that the spectral features associated with localized electronic densities, like two-center interference [32, 36, 40, 47, 48, 49, 50, 51, 52, 53] or Cooper-like minima [35, 54, 55, 56, 57, 58], are good references for tracking the migrating dynamics.

This paper is organized as follows: In Section 2 we review the information content in high-harmonic spectra and outline how to interpret signals that directly correspond to the molecular electronic structure. In Section 3 we present HHS results of two-center interferences and Cooper-like minima in small molecules. We then examine carbonyl sulfide, which exhibits both, to explore methods to deconvolve signals originating from both. We follow these results with a brief discussion of how these structural features could be leveraged to view a time-dependent charge migration. In Section 4, we look at semi-classical and first principles-based methods for modeling HHS. Within the first principles methods, we discuss how one can isolate the short-trajectory contribution in single-target simulations of HHG, which provides a sub-cycle view of the electron migratory dynamics. In Section 5 we expand our scope to emphasize other efforts that will be needed to employ HHS for probing charge migration, such as direct computation of electron dynamics and ionization spectroscopy. We summarize in Section 6.

2. Molecular high-harmonic spectroscopy

In order to harness HHS for measuring charge migration one needs to (i) fully characterize the spectral amplitude and phase of the harmonic emission and (ii) isolate signals that are unique to the system's electronic structure from other generic contributions found in any system that emits high-harmonics. In this section, we discuss experimental and theoretical approaches to achieve this. We first outline experimental methods for measuring molecular-frame HHS amplitudes and phases. Then, we discuss the theoretical approach for modeling molecular high-harmonic spectra, highlighting the different contributions to the signal. Finally, we show how to separate generic from target-specific contributions in HHS.

2.1. Experimental methods and apparatus

HHS enables simultaneous multidimensional measurements, involving the acquisition of both spectral amplitudes and phases with molecular-frame resolution. All experimental results discussed in this review were obtained using a mid-infrared (mid-IR) tunable wavelength driving laser source for the generation and characterization of the extreme-ultraviolet (XUV) harmonics, as well as impulsive alignment of the molecular target [59]. Impulsive alignment allows for control over the angle between the driving laser polarization and the molecular axis. Compared to conventional near-IR measurements, the mid-IR source gives access to a broader range of XUV harmonics because of the quadratic scaling of the harmonic cut-off with the laser wavelength and a finer harmonic sampling [43, 44, 60, 61].

For all measurements described in this review, the spectral amplitude of the harmonic emission is recorded using an XUV photoionization magnetic bottle electron spectrometer. The phase retrieval is performed using the reconstruction of attosecond beating by interference of two-photon transitions (RABBITT) method [62, 63]. The RABBITT apparatus consists of a Mach-Zehnder interferometer where the majority of the laser power is in one arm and is used for high-harmonic generation. The resulting XUV radiation is sent through an aluminum filter to remove the mid-IR beam. The trasnsmitted XUV radiation is then recombined with the dressing laser beam (from the other arm of the interferometer) using a hole drilled in a mid-IR reflecting mirror. The overlapping XUV radiation and mid-IR dressing beam are then focused, using a gold coated toroidal mirror, into the magnetic bottle electron spectrometer. All recorded spectral information is corrected for the contributions from the aluminum filter transmission and the detection gas photoionization cross-section used in the electron spectrometer.

All measurements discussed here were taken with tunable mid-IR, 60-75 fs pulses produced by pumping a commercial optical parametric amplifier (OPA; HE-TOPAS Prime, Light Conversion) with a chirped-pulse-amplified Ti:sapphire system, at a 1-kHz repetition rate. The OPA produces approximately 1 mJ pulses whose energy can be attenuated with a half waveplate, polarizer combination. For molecular-frame measurements, such as those described in 3.1 and 3.3, the depleted pump of the OPA is used to induce impulsive molecular alignment. The alignment pulse propagates parallel to the HHG driving beam and has a variable delay with respect to it. Additionally, a half waveplate is placed in the alignment pulse beam path for polarization control. Additional details of the experimental apparatus can be found in [35, 36].

2.2. Molecular high-harmonic spectrum

HHS is an application of high-harmonic generation, a three-step non-linear process where a strong field incident upon an atomic or molecular target (i) creates an electron wavepacket in the continuum via tunnel ionization, (ii) accelerates the electron wave packet, and (iii) returns it to its parent ion [43, 44, 45, 46]. Upon recollision (iii), a transient dipole coherence between the returning wave packet and the bound molecular wave packet leads to the emission of harmonic radiation. In the three-step picture, HHS takes advantage of the intrinsic coherence of the harmonic process – the same electron that is ionized in (i) is later involved in the recollision (iii) and associated emission – to probe the ion. Finally, because the harmonic emission is tied to the bound electron wave packet, HHS signals contain information on the molecule's or atom's structure at the moment of recollision [33, 34].

Because of the different time, length, and energy scales involved in the three successive steps of HHG, the harmonic spectrum produced is simply the product of the cross sec-

tions and respective phase dependencies from each step individually: the probability to first ionize an electron, times the probability for that electron wave packet to recollide, times the efficacy of the harmonic emission process. For a time-independent charge density of the ion, this factorization can be performed directly in the frequency domain, an approach known as quantitative rescattering theory (QRS) [64]. Formally, this results in a formula for the harmonic spectral amplitude given by [65, 66, 67],

$$HHG(\nu;\theta) = \sqrt{\frac{\Gamma(\theta)}{\Gamma_{ref}}} \times HHG_{ref}(\nu) \times \sigma(\nu;\theta) e^{i\phi(\nu;\theta)}, \quad (1)$$

where ν is the harmonic frequency and θ is the molecular orientation/alignment angle. Here Γ is the energy-independent ionization yield, and σ and ϕ are the scattering amplitude and phase, respectively. In this electron-scattering context, the amplitude corresponds to the recombination dipole matrix element (RDME),

$$\sigma(\nu;\theta) e^{i\phi(\nu;\theta)} = \left\langle \psi_b \left| \hat{d} \right| \psi_c \left(\vec{k} \right) \right\rangle, \quad \nu = \frac{\left| \vec{k} \right|^2}{2} + I_p, \quad (2)$$

where ψ_b and ψ_c are the neutral and singly-ionized (with scattering momentum $\vec{k}(\theta)$) wave functions, respectively, $\hat{d}$ is the dipole/acceleration operator, and I_p is the target's ionization potential. Finally, as systems that share the same ionization potential will also share many generic amplitude and phase features in the emitted radiation (assuming tunnel ionization dominates [67]), HHG_{ref} of Eq. (1) is a normalized reference spectrum with ionization yield Γ_{ref}, generally associated with an atomic target with matching ionization potential and a featureless scattering phase,

$$HHG_{ref}(\nu) = \frac{HHG_{atom}(\nu)}{\sigma_{atom}(\nu) e^{i\phi_{atom}(\nu)}}. \quad (3)$$

Alternatively, when studying aligned or oriented molecular samples one can also self-reference the spectral amplitude to an unaligned sample, or to the signal at a molecular alignment angle that has a featureless spectral amplitude [36].

Overall, HHS aims to isolate the target-specific amplitude σ and phase ϕ and uniquely connect them to the molecule's electronic structure [18, 37, 66]. Of these components, the spectral amplitude is the simplest to isolate. From Eq. (1) we directly see that one only needs to normalize against the reference spectrum. On the other hand, as discussed in Section 2.1, measuring spectral phases in molecules is more difficult than amplitudes, and hence only a few measurements have been made [35, 36, 39, 50, 68]. Isolating the target-specific spectral phase is further complicated because the reference spectrum, despite having a featureless RDME, still has a variable spectral phase, known as the attochirp [69]. This attochirp typically dominates over the target-specific phase contribution of interest and hence is not easily removed [69, 70]. A full complex characterization of the target-specific signal, however, is necessary for HHS studies as the amplitude alone cannot distinguish the multiple contributions that the RDME may have. This point is further illustrated in Section 3.3.

Instead of directly measuring the harmonics' phases, the RABBITT method (see Section 2.1) measures their derivatives with respect to frequency, *i.e.*, the group delay (GD). From Eq. (1), the group delay is split into the attochirp and the target-specific RDME contributions

$$GD_{HHG}(\nu;\theta) = GD_{ref}(\nu) + GD_{RDME}(\nu;\theta). \quad (4)$$

To a good approximation, the group delay can be interpreted as the relative time τ at which a given harmonic is generated. Using a semi-classical framework, the attochirp can further be approximated using the three-step model and assuming the propagating free electron wavepacket does not experience the ion's potential [35, 43, 44, 66]

$$GD_{ref} \approx GD_{free} \approx \tau_{free}. \quad (5)$$

This factorization and approximation has been validated for atoms [69, 70, 71, 72, 73] and small molecules [35, 36]. For larger molecules however, the validity of the factorization is unclear due to the non-negligible spatial extent of the molecular potential. Therefore, self-referencing in molecules is expected to be the more robust approach.

For charge migration studies, the generalization of the QRS factorization of Eq. (1) is not obvious due to the ultrafast time-scale associated with the migratory dynamics. The picture can be further complicated if multiple ionization channels, with different ionization potentials, are involved in the migration process. Nevertheless, in the context of the three-step model, charge migration does not begin until after the ionization step, and hence the technique of (self) referencing the harmonic signal in order to extract time-dependent target-specific signatures of the dynamics still remains valid. Accordingly, we propose that otherwise static features in the spectral amplitude and phase, *e.g.*, two-center interferences [32, 36, 40, 47, 48, 49, 50, 51, 52, 53] or Cooper-like minima [35, 54, 55, 56, 57, 58], provide good points of reference for charge-migration studies: deviations from the static reference would serve as a signature of transient reorganization of the target's electronic structure. This concept is further developed in Section 3.

2.3. Attochirp removal

As discussed in the previous section, access to target-specific spectral information requires first the removal of the generic attochirp contribution to the signal. If the ionic potential is negligible during propagation, the attochirp is a parametric function of the target's ionization potential and several laser parameters [45]. Unfortunatley, laser intensities are not typically measurable to high precision. Instead, we assume the contribution from the RDME is negligible compared to the attochirp in Eqs. (4-5),

$$\left| GD_{RDME} \right| \ll \left| \tau_{free} \right| \quad \Rightarrow \quad GD_{HHG} \approx \tau_{free}, \quad (6)$$

so the intensity can be recovered by fitting against the measured group delay spanning a broad energy range. The accuracy of the intensity retrieval, using a weighted least-squares

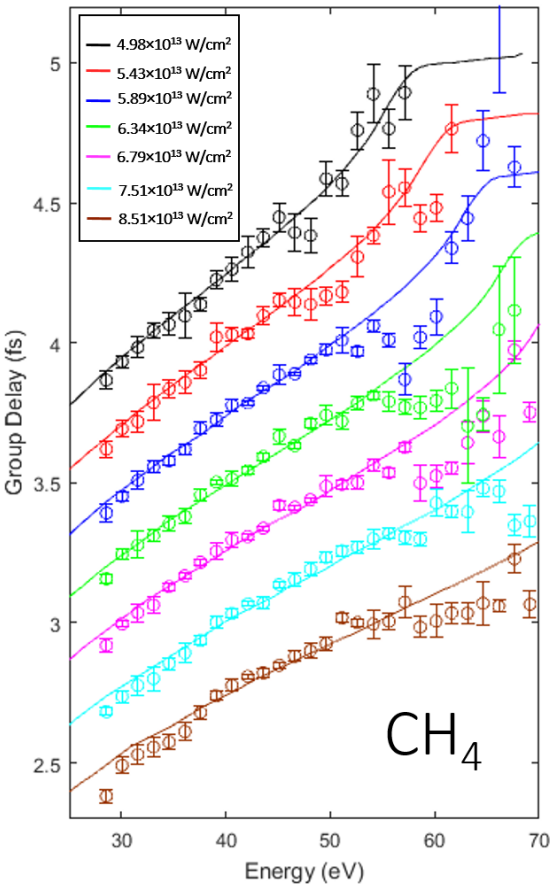

Figure 1: Illustration of the laser intensity fit for the attochirp removal discussion in Section 2.3. Measured group delays are shown in circles with the calculated attochirps for each intensity given as solid lines. Each intensity was offset by 0.2 fs when plotting for visual clarity. Additional details about the experiment and measurements can be found in [35]; licensed under a Creative Commons Attribution (CC BY) license.

minimization algorithm, was confirmed in xenon [35], where the assumption of a negligible ionic potential is known to be valid [70].

The intensity retrieval for a molecule with a featureless RDME is illustrated in Fig. 1. The figure compares the measured group delay for methane with the calculated attochirp for a 1650 nm driving wavelength at varying laser intensities. The attochirp calculation was performed for the lowest intensity dataset and then scaled with the measured laser power for the others. Indeed, keeping the focal geometry unchanged, the (unknown) laser intensity scales linearly with the power, which is readily measured. Fig. 1 shows excellent agreement between the measurement and calculated attochirp over an intensity range of 5 to 8.5 $\times$ 10^{13} W/cm^2 [35].

HHS and its application for charge migration studies involve measurements for which the target-specific group delay is not negligible. The presence of an additional contribution to the group delay besides the attochirp will impede the intensity retrieval, and hence the attochirp subtraction. To circumvent this issue, the intensity can first be calibrated in a reference molecule with a negligible target-specific group delay. The calibrated intensity can then be used to compute the attochirp component in the target of interest to reveal its target-specific group delay signal. This intensity calibration method was used to study the Cooper-like minimum in methyl chloride (CH_3Cl), in Section 3.2.

3. Experimental molecular high-harmonic spectroscopy

Utilizing the methods outlined in Section 2, we now present characterizations of two molecular structural features caused by the ion's charge distribution, which might be leveraged as references for charge migration studies: two-center interferences and Cooper-minima. We then examine the characterization of a molecule that exhibits both types of structural features, illustrating the need for multidimensional measurements of both amplitude and phase to deconvolve the contributions from each feature in the emitted radiation. We briefly extend the discussion to how one would use a similar approach to deconvolve a static feature, such as a two-center interference or Cooper minima, and a dynamic feature, resulting perhaps from charge migration.

3.1. Aligned target - Two-center interference

The simplest spectral feature found in molecular HHG spectra, but absent in atoms with the same ionization potential, are those due to two-center interferences. These are a direct result of the localization of charge at multiple sites within a molecule [47]. Two-center interferences have been observed experimentally and theoretically in multiple systems [32, 40, 48, 49, 50, 51, 52, 53]. In a small molecule where the highest occupied molecular orbital (HOMO) is mainly composed of two roughly symmetric charge density centers, the scattering of a recolliding electron wave packet from each center leads to energy-dependent constructive and destructive interferences. These target-specific features also depend on the molecular alignment angle relative to the driving laser polarization. Accordingly, without known molecular alignment, one cannot directly access the target specific RDME.

In two-center molecules, upon recollision, the returning electron wave packet scatters off each center. Therefore, conceptually, if the bound wave function is written as a linear composition of the atomic orbitals of the centers, $\psi_b = \psi_b^1 + \psi_b^2$, then the RDME of Eq. (2) becomes

$$\left\langle \psi_b \left| \hat{d} \right| \psi_c \right\rangle = \left\langle \psi_b^1 \left| \hat{d} \right| \psi_c \right\rangle + \left\langle \psi_b^2 \left| \hat{d} \right| \psi_c \right\rangle . \quad (7)$$

If the two centers are roughly symmetric, *i.e.*, they have similar charge density, then assuming the recolliding electron wave packet is a plane wave, the condition for a destructive interference minimum is [74]

$$k_e R \cos\theta + \Delta\Phi(k_e, \theta) = (2m+1)\pi \quad (8)$$

where $k_e = 2\pi/\lambda_e$ is the electron wave number, λ_e is the electron de Broglie wavelength, R is the effective distance between the two centers, θ is the angle between the molecular axis and plane wave k-vector, $\Delta\Phi$ is the RDME phase difference between the two centers, and m is any integer.

In the two-center interference framework of Eqs. (7-8), the three main molecular characteristics that determine the feature are (i) the relative distribution of charge between the two centers, (ii) their spatial separation R, and (iii) the phase difference $\Delta\Phi$ between them. The relative distribution of charge between the two centers controls the sharpness of the minimum, with a symmetric distribution yielding the strongest interference. The separation of the charge centers and the relative phase between them then determines the energy at which the minimum occurs, as well as its angular distribution. Note that Eq. (8) only gives a conceptual understanding of two-center interference minima since plane waves are not necessarily a good approximation for continuum wave functions [36].

Fig. 2 shows an example of HHS of the two-center interference in CO_2. The inset of panel (c) shows the isosurface of the HOMO, with the dominating linear combination of atomic orbitals (LCAO) composition. The symmetric distribution of charge around the two oxygen centers leads to the two-center interference in the harmonic spectrum. Panel (a) shows that the two-center minimum continuously moves to higher harmonic energy as the absolute value of the angle θ (upper x-axis) between the molecular axis and the driving laser polarization increases from zero. Here θ is controlled through the delay between the alignment and harmonic generation pulses (lower x-axis) near a half revival of the rotational wave packet [75, 76]. Alternatively, θ can be controlled by fixing the delay at the half revival and rotating the polarization of the alignment pulse. The latter method is used for the target-specific spectral intensities and group delays of panels (c-d). Because the angular variation occurs over a very short time period compared to the revival time there is no significant spreading of the rotational wave packet and both methods yield similar results [36].

Fig. 2 (b) illustrates self-referencing in molecular HHS by normalizing the alignment-angle-dependent spectral intensity to that at 90°. Indeed, at perpendicular alignment the predicted two-center minimum of Eq. (8) moves beyond the harmonic cut off. Experimentally, the near-featureless nature of the spectrum at $\theta = 90°$, and therefore its suitability as a normalization reference, is confirmed by the flatness of the normalized signal from an unaligned sample in which the contributions from all different alignment angles washes out the interference minimum (see the discussion in the next subsection). The only remaining trace of the minimum is the dampened yield at higher energies. This is understood as a macroscopic effect where the ensemble of alignments in the unaligned sample are out of phase over a large range of energies due to the energy-dependent phase shift [36]. Fig. 2 (c) shows that the angle-dependence of the group delay feature is consistent with that of the amplitude. Both show a local minimum near the same energy for aligned samples, which moves to higher energy with increasing alignment angle, and the unaligned sample shows a flat group delay. This angle dependence is consistent with Eq. (8) and with the fact that the phase difference between the two centers is independent

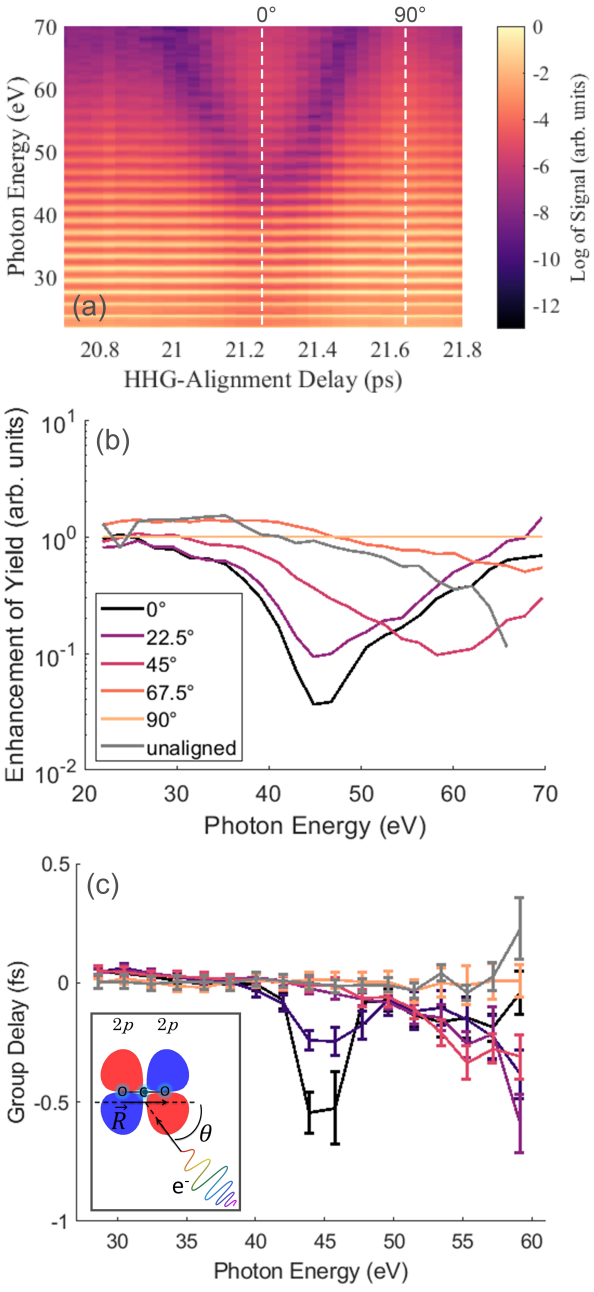

Figure 2: Experimental high-harmonic spectroscopy of the two-center interference in CO_2. (a) Harmonic yield as a function of alignment angle (upper x-axis) as controlled by the alignment pulse delay relative to the HHG pulse (lower x-axis). (b) Enhancement of HHG yield when self-referenced against the 90° spectrum, as outlined in Section 2.2. (c) Associated group delays with the attochirp subtracted as outlined in Section 2.3. (inset) Isosurfaces of the HOMO with red and blue indicating opposing phases, and the dominating LCAO composition written above. Reproduced from [36], with the permission of AIP Publishing.

of alignment, with $\Delta\Phi(\theta) = \pi$, as shown on the isosurface in the inset. Intuitively, increasing θ decreases the effective two-center distance and therefore pushes the minimum to higher energies. Qualitatively similar results were obtained in N_2O [36], which further confirms that two-center interferences are observable in HHS whenever the molecule has two roughly symmetric charge density centers.

Because a two-center interference is a direct consequence of localized electronic charge distributions, it lends itself as a promising static reference for charge migration studies. Assuming measurements have access to a clear temporal dimension, *e.g.*, by controlling the sub-cycle delay between the harmonic generation field and the migration dynamics, an oscillation of charge along the molecule would induce a periodic reshaping of the minimum. Assuming that the conceptual model presented in Eqs. (7-8) holds and can be extended to include migration dynamics in the bound wave function ψ_b, the time-dependent sharpness of the minimum would reflect the relative charge asymmetry between each center, while the sign of the group delay would be sensitive to which center had a greater charge density [25].

3.2. Unaligned target - Molecular Cooper-like minimum

In an unaligned sample one measures the coherent average of the harmonic emission over all possible orientations. From Eq. (1), the effective RDME of an unaligned target is

$$\sigma_u(\nu)e^{\phi_u}(\nu) = \frac{\int \sqrt{\Gamma(\theta)}\sigma_{target}(\theta;\nu)e^{\phi_{target}(\theta;\nu)}d\theta}{\int \sqrt{\Gamma(\theta;\nu)}d\theta}. \quad (9)$$

This coherent averaging, as was previously seen in Section 3.1, typically supresses any two-center interference signal as the contributions from each angle destructively interfere in the observed signal. However, not all unaligned molecules have a featureless RDME. Molecules with a significant charge density centered around one atom can have angle-independent features, such as a Cooper minimum, that are due to the electronic structure.

A Cooper minimum [54] is a minimum in the photoionization cross section at a specific photon energy. When an electron of effective angular momentum ℓ is single-photon ionized, it has two angular momentum pathways ($\ell \rightarrow \ell \pm 1$) into the continuum. A zero transition dipole matrix element in one of the channels at a specific energy can hence yield a Cooper minimum in the photoionization cross section, even though it is an incoherent sum over the pathways. Since HHS probes the RDME, which is the inverse of the single-photon ionization process, the Cooper minimum appears as a minimum in the emitted radiation as well. One important difference is that HHS involves a coherent sum over the angular momentum channels, which can shift the energy that it appears at. Originally observed in alkali atoms [55] and later observed in small molecules [56, 57, 58], Cooper-like minima can be found in some molecules that have a significant localized charge density around an atomic center. In contrast to the two-center interference discussed in Section 3.1, the Cooper minimum is not an interference effect and is a feature of a single charge center giving rise to the angular-independence.

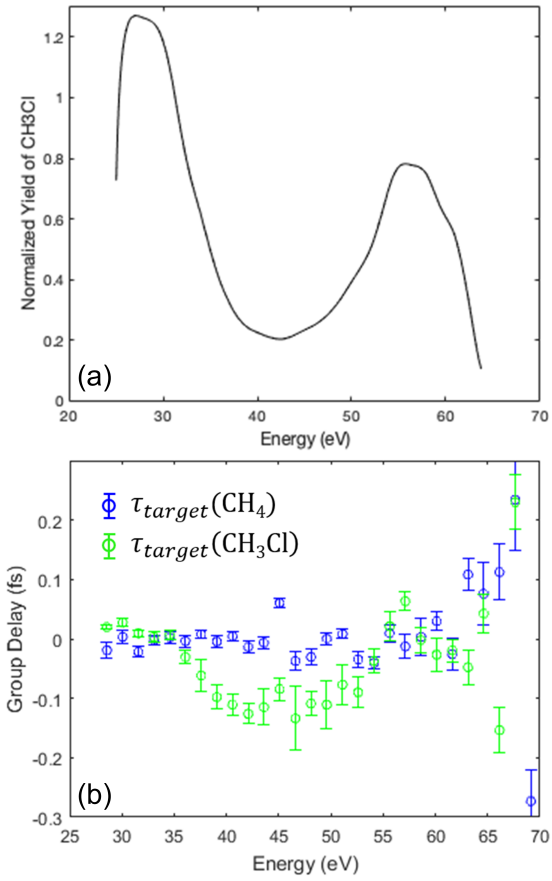

Figure 3: Influence of the methyl chloride Cooper-like minimum in reference to methane. (a) HHG yield normalized to a methane spectrum taken at the same intensity, as outlined in Section 2.2. (c) The associated group delays with attochirp subtracted as outlined in Section 2.3. Additional details about the experiment and measurements can be found in [35]; licensed under a Creative Commons Attribution (CC BY) license.

Fig. 3 shows the results of a HHS measurement for the Cooper-like minimum in methyl chloride (CH_3Cl). The Cl p orbital accounts for approximately 80% of the HOMO, with the C-Cl bond filling out the shell [56]. The Cooper-like minimum thus arises since the d-like channel from the Cl charge center has a zero in its matrix element. The target-specific spectral intensity and group delay are extracted using methane, which differs from methyl chloride solely by a chlorine substitution, as a reference. The Cooper-like minimum influences both the spectral amplitude and group delay around 42.4 eV, consistent with other chlorinated molecules [77]. The results are analogous to observations in argon, which has a Cooper minimum associated with the $3p$ orbital [33, 78] that has a very similar structure to the HOMO of methyl chloride [56, 79].

3.3. Unraveling multiple features

So far we have considered how single, well-identified features shape the target-specific HHS signal. However, HHS measurements associated with charge migration studies will likely convolve features reflecting multiple characteristics of the target molecules. In a time-independent context, a similar mixing of features can be observed in OCS where the spectral amplitude and phase are determined by the interplay between a geometric two-center interference and a structural Cooper-like minimum [36].

HHS measurements in OCS are shown in Fig. 4. The OCS HOMO shown in the inset of panel (b) has charge density distributed between two centers with a π phase difference between centers, qualitatively similar to that for CO_2 – see Fig. 2. Specifically, the $2p$ orbital of oxygen and the $3p$ orbital of sulphur make up 97% of the HOMO, with the C-S bond filling out the shell [80]. Thus, OCS is isoelectronic with methyl chloride. Accordingly, it has a Cooper-like minimum that is clearly observed in HHS from an unaligned sample with a dip in the spectral amplitude and group delay around 42 eV (as shown in panels (a) and (b)). Any two-center interference feature is washed out in the unaligned sample, therefore isolating the Cooper-like minimum in the energy resolved signal [36].

Unlike the Cooper-like minimum, the two-center interference in OCS is hard to observe. Because the Cooper-like minimum component is present at all angles, what is measured is its convolution with the two-center interference [36]. In Fig. 4, this combination manifests as a spectral feature that appears at the same harmonic energy for all alignment angles with only a variation of the sharpness of the intensity minimum and the sign of the group delay. In a simplified additive picture, the angle-independent Cooper-like minimum provides an energy window within which the effect of the two-center interference can be observed. For alignment angles where the two features' extrema overlap, the coherent interference between them produces sharp features, with nontrivial θ dependence. When the extrema are not overlapped in energy, each component minimum is occluded by the other stronger signal, leading to the quasi-flat spectral signal for $\theta = 90°$. The complex interplay between the two-center and Cooper-like features is further discussed from a theoretical perspective in Section 4.1.

OCS exemplifies the crucial importance of multidimensional analyses for HHS campaigns. The contribution and interplay of geometric two-center interferences and structural Cooper-like minima is revealed only after comparing simultaneous multidimensional measurements of both the target-specific spectral amplitude and phase, in both aligned and unaligned samples. Returning to the case for using HHS to study charge migration discussed at the end of Section 3.1, OCS showcases the importance of exploiting reference features in harmonic spectra. For instance, if we imagine charge migration dynamics convolved with a static structural feature, then time-dependent variations in the HHS signal around the static feature would represent a high-resolution signature of the charge migration. Additionally, as these static reference features appear as minima in the HHS signal, they have a lower threshold for revealing any additional signal contributions and therefore should be most sensitive to the migratory variations in the electronic structure.

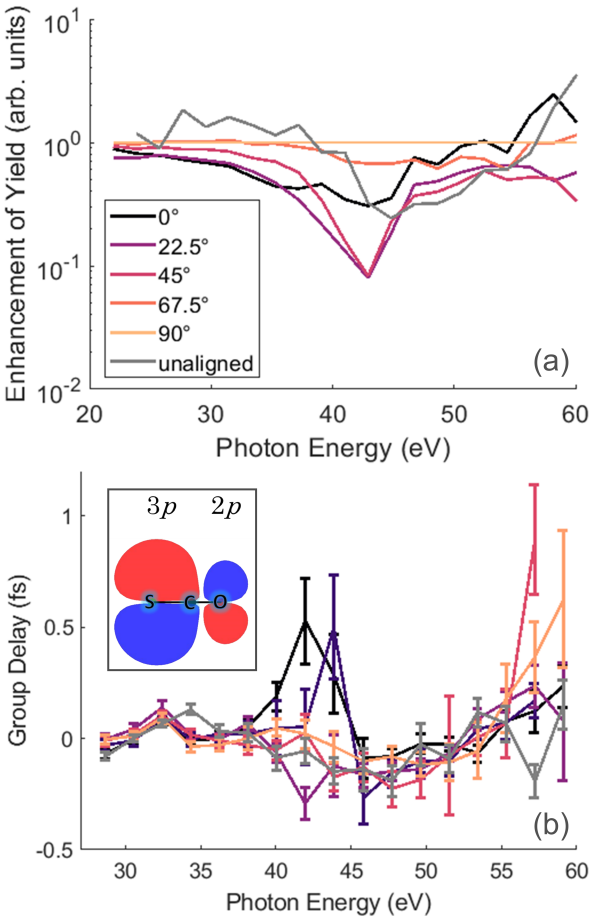

Figure 4: Spectral intensities and group delays for OCS. (a) Enhancement of HHG yield when self-referenced against the respective $\theta = 90°$ spectra, as outlined in Section 2.2. (b) Group delays for each respective molecule. The attochirp was subtracted from the group delay figures, as outlined in Section 2.3. Group delay data above 60 eV was omitted due to poor statistics from low count rates. (inset) Isosurface of the HOMO orbital with red and blue indicating opposing phases, and the dominating LCAO composition written above. Reproduced from [36], with the permission of AIP Publishing.

4. Theoretical molecular high-harmonic spectroscopy

Charge migration was first identified theoretically [1] and calculations continue to play a key role in both understanding the complex process and identifying preferred experimental targets and methods [18, 25, 81]. Numerically, simulating HHS with complex molecules is an extremely difficult and resource-intensive task as it requires the accurate description of both (i) the multi-bound-electron structure close to the core and (ii) the energetic electron in the continuum. Practically, various approaches have been developed for HHS

simulations, including (semi-classical) factorizations based on the three-step model and direct numerical simulations. We introduce examples of these, and discuss their strengths and limitations for charge-migration studies, in Sections 4.1 and 4.2, respectively.

Meaningful comparison of HHS simulations with experimental signals are further complicated by the disparity between the microscopic single-molecule response to the strong laser field versus the measured macroscopic response [27, 70, 82]. Specifically, single-molecule harmonic generation consists of multiple possible quantum trajectories. As a result, multiple ionization times and their corresponding recollision times result in the same harmonic energies [45]. All of these trajectories interfere in the overall signal, but only one of the energy-degenerate trajectories, the so-called short trajectory, survives the macroscopic phase matching and focal-volume averaging present in experiments [83]. We discuss a method for isolating the short-trajectory contribution in single-target simulations in Section 4.2.1 and explore its efficacy upon comparison with measurement in Section 4.2.2. Alternatively, direct simulation of the macroscopic response [83, 84] involves the computation of many single-molecule responses and would therefore be extremely computationally expensive given that an individual harmonic calculation is already taxing.

Finally, the control offered by theoretical methods in short-trajectory selection allows for sub-cycle resolution not currently achievable in measurement. This resolution provides key insight into the effect of the driving field on electron dynamics, normally modeled as field-free, which is illustrated in Section 4.3.

4.1. Recollision-factorization models

To simulate molecular high-harmonic generation, some models leverage the factorization of the three-step process into its (i) ionization yield, (ii) rate of recollision, and (iii) recollision cross-section. Depending on the specific approach, this factorization can be done in the temporal domain, employing a semi-classical approach such as the stationary-phase approximation [45], or it can be performed directly in the frequency domain as with QRS [43] – see discussion in Section 2.2. In temporal-domain factorizations and associated semi-classical models, which provide direct access to the recollision temporal information, the short-trajectory selection can be performed at the microscopic level by accordingly discarding all but these contributions to the overall factorized signal [85]. For frequency-domain factorizations, a similar selection can be achieved by ensuring that the reference term, HHG_{ref} of Eq. (1), itself only contains short-trajectory contributions or has been macroscopically filtered [67]. Additionally, for charge migration studies, temporal-domain approaches can be augmented to include a time-dependent charge density [19]. Irrespective of the specific approach, recollision-factorization-based models typically involve many parameters associated with the different factors, and can therefore be hard to calibrate.

Examples of recollision-factorization models, in the frequency domain, are shown in Fig. 5. These models are built using a qualitative approach to the QRS of Eq. (1) and are developed for conceptual analyses of experimental measurements (markers) in CO_2 and OCS (left and right panels, respectively) otherwise discussed in Sections 3.1 and 3.3. Specifically, these models aim to recreate both the amplitude and phase of the emitted radiation and are designed to include the effects of structural features, such as two-center interferences and Cooper minima, and accurately predict the location, magnitude, and, most importantly, the alignment angle dependence of each. Briefly, the ionization yield $\Gamma(\theta)$ is fitted against the total experimental harmonic signal, and HHG_{ref} is chosen as a suitable featureless reference. For CO_2, the two-center interference is modeled with a Gaussian-shaped geometric feature, in both the RDME amplitude σ and phase ϕ, that moves in energy upon variation of the molecular alignment. For OCS, the geometric two-center interference is augmented with an alignment-angle-independent Cooper-like minimum contribution. Additional details about the models, and their calibration against experiments, can be found in [36].

Overall, Fig. 5 shows a very good agreement between the conceptual recollision-factorization model and experiments. For CO_2 (left panels), upon alignment the two-center interference manifests as an angle-dependent dip in both the HHS intensity (top) and target-specific group delay (middle) which is mostly washed away for unaligned molecular samples (top inset and bottom panel). On the other hand, with OCS the position in energy of the minimum in the total harmonic signal is independent of alignment, with only the depth of the intensity minimum and sign of the group-delay varying. However, in accordance with experiment, unlike CO_2, unaligned OCS samples preserve a clear local minimum in the harmonic intensity and target-specific group delay due to the Cooper-like minimum.

Taken together, the results of Fig. 5 offer valuable insight for molecular HHS. For aligned CO_2, it shows that the energy of the two-center minimum moves with alignment as

$$\nu_{\min} \approx I_p + \frac{\alpha}{|\cos\theta|^{\beta}} \tag{10}$$

with $\beta \approx 1$ instead of predicted $\beta = 2$ from the recollision-plane-wave approximation of Eq. (8). This difference highlights the importance of using accurate RDMEs in QRS factorizations [36]. For unaligned CO_2, the two-center interference is averaged away, as discussed in Section 3.1. This also confirms the potential of using the unaligned signal as a molecular self-reference for extracting target-specific spectral information. For OCS, the unaligned and angular-dependent signals are the results of the interplay between the geometric two-center interference and structural Cooper-like minimum features, as discussed in Section 3.3, and hence it exemplifies the profound reshaping of HHS signals when multiple contributions overlap and interfere. Notwithstanding the insights gained from these specific cases, this conceptual model illustrates the complexity and potential limitations of recollision-factorization approaches as they require knowl-

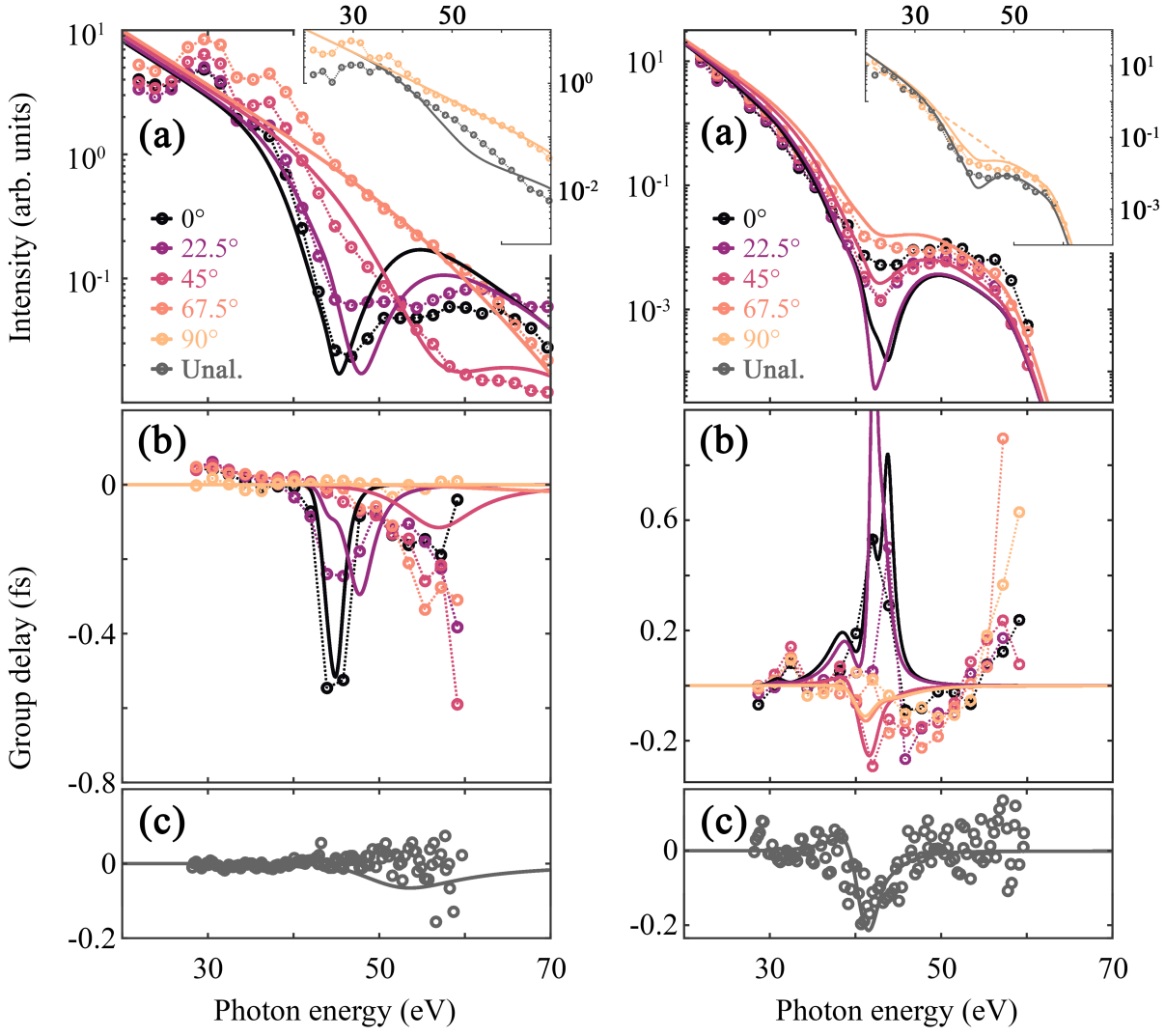

Figure 5: Illustration of recollision-factorization models (curves) and comparison with experimental measurements (markers). In the QRS framework of Eq. (1) the CO_2 conceptual model (left panels) includes a generic two-center interference feature both in the RDME amplitude and phase. For OCS (right panels), the model is augmented with an angle-independent Cooper-like minimum feature. Reproduced from [36], with the permission of AIP Publishing.

edge of the number of features present and their angle dependencies in addition to multiple empirical parameters.

4.2. Direct numerical simulations

Molecular HHS can also be investigated using first-principles simulations. For instance, time-dependent density-functional theory (TDDFT) has shown promising results on simulating experimental HHS results recently [25, 36, 86, 87, 88, 89]. In essence, these direct numerical simulations remove the many parameters involved in their factorization counterparts, at the price of being generally more computationally expensive. Conversely, because they do not decompose the harmonic-generation dynamics into distinct processes, first-principle simulations can be more challenging for separating multiple contributions to the harmonic signal. More importantly for HHS, in direct numerical simulations, proper selection of the short-trajectory signal in single-molecule simulations requires careful attention, as discussed next.

4.2.1. Short-trajectories selection with an attosecond pulse train seed

Numerically, the contribution from short trajectories to the harmonic spectrum can be selected spatially by taking advantage of the fact that other unwanted quantum orbits travel larger distances from the core. This, however, requires high-performance absorption of outgoing electron fluxes at the edges of the simulation domain in order to avoid any spurious reflection that would pollute the short trajectory harmonic signal. Crucially, the position of these absorbers needs to be carefully calibrated, specific to the target and laser parameters, which can make it an impractical approach for first-principle HHS simulations. A different approach for short trajectory selection that avoids filtering of the long trajectories is to avoid producing long trajectories to begin with using a weak attosecond-pulse-train (APT) ionization seed [25, 90, 91] synchronized to the driving mid-IR laser field,

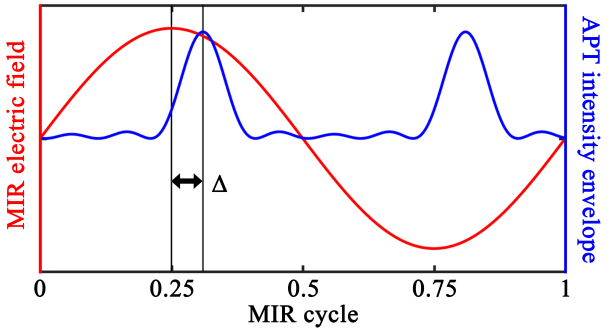

Figure 6: Illustration of the APT ionization seed for selecting short trajectories in single-molecule simulations. The APT pulse (right axis) is synchronized to the driving mid-IR (left), with a delay Δ set to selectively enhance ionization of the short-trajectory contributions to the harmonic signal [67]; licensed under a Creative Commons Attribution (CC BY) license.

as illustrated in Fig. 6. By properly timing the APT with respect to the part of the mid-IR sub-cycle when short trajectories are initiated, their contribution to the harmonic signal is selectively enhanced and dominates over other quantum orbits. More details about calibrating the APT ionization seed for molecular HHS can be found in [36].

As is usual, the harmonic signal is computed from the Fourier transform $\mathcal{F}$ of the total dipole or acceleration response [85]. For targets that do not exhibit an inversion symmetry, alignment-only harmonic signals are obtained by coherently averaging the responses from opposite orientation angles θ and $\theta + \pi$. The extraction of the short-trajectory signal can be further improved by windowing the response around a single set of APT-enhanced recollision times. The harmonic intensity associated with the dipole acceleration $\mathbf{a}(t)$ then reads

$$|\, HHG(\nu,\theta)\,|^2 = |\, \mathcal{F}[W(t)a_{\parallel}(t,\theta)]\,|^2 + |\, \mathcal{F}[W(t)a_{\perp}(t,\theta)]\,|^2, \tag{11}$$

where $W(t)$ is the recollision window function. Note that, selecting a single set of short-trajectory recollision times yields a continuous spectrum in lieu of the experimental discrete harmonic comb [25]. Additionally, because of the anisotropy of molecules, the harmonic component perpendicular to the laser polarization may not vanish and should therefore be accounted for in the total intensity [85].

As with experimental measurements, extracting the target-specific group delay is more involved than the spectral intensity and requires a featureless reference. From the QRS factorization of Eq. (1), the group delay is given by

$$GD_{RDME}(\nu;\theta) = -\frac{\partial\phi}{\partial\nu} = -\frac{\partial}{\partial\nu}\arg\left(\frac{HHG(\nu;\theta)}{HHG_{ref}(\nu)}\right). \tag{12}$$

The reference spectrum can be computed with a single-active-electron Schrödinger-equation atomic model with matching ionization potential and subjected to an identical total laser field, including the APT ionization seed [25]. Including the APT field helps mitigate systematic spectral features it might induce in the harmonic spectrum. Practically, the reference computation can be performed in reduced dimension, with one- and two-dimensional references yielding essentially identical results [25]. Finally, like for the spectral intensity, both parallel- and perpendicular-to-the-laser polarization direction contributions should be included in the total group delay with the following weighting

$$GD = \frac{\left|\mathcal{F}[Wa_{\parallel}]\right|^2 GD_{\parallel} + \left|\mathcal{F}[Wa_{\perp}]\right|^2 GD_{\perp}}{\left|\mathcal{F}[Wa_{\parallel}]\right|^2 + \left|\mathcal{F}[Wa_{\perp}]\right|^2}. \tag{13}$$

More details about the computation of the spectral intensity and target-specific group delay can be found in [25].

4.2.2. *high-harmonic spectroscopy simulations with time-dependent density-functional theory*

Practically, one of the main limiting factors in first-principles direct numerical simulations of molecular harmonic spectra is the computational cost of each simulation. Time-dependent density-functional theory (TDDFT) offers somewhat reasonable complexity scaling with the number of active electrons, and among TDDFT implementations, because of the high energy and large excursion of the recolliding electron from the core, grid-based methods seem best suited to carry out such simulations. All TDDFT computations reviewed in this section are carried out with the grid-based package OCTOPUS [92, 93], using a local-density approximation (LDA) exchange-correlation potential [94, 95, 96, 97] and average-density self-interaction correction (ADSIC) [98]. The driving mid-IR field has 60-TW/cm^2 intensity and 1500-nm wavelength, while the APT-ionization seed is set to $1-2\%$ of the intensity of the mid-IR. Corresponding alignment-angle dependent spectral intensity and group delay for CO_2 and OCS are shown in Fig. 7. More details about these TDDFT simulations, and detailed comparison with experimental measurements, can be found in [25].

Overall, Fig. 7 highlights both the success and limitations of current state-of-the-art TDDFT simulations using an APT seed for semi-quantitative description of molecular HHS. In all panels, we see that any individual computation (each vertical slice of the colormaps) is hard to interpret while trends in the aggregated alignment-angle dependent signals reveal very clear and distinctive patterns. Most strikingly in Panel (a), the spectral intensity for CO_2 shows a clear minimum that moves to higher harmonic energies as the molecular alignment is varied in accordance with experiment. Interestingly we see that the empirical angle dependence of the two-center interference minimum of Eq. (10) is also well captured by the simulations, as indicated with the parabolic black curve, and matches experimental results discussed in Section 3.1.

Alternatively, in Panel (b), the spectral intensity for OCS shows qualitative differences with its experimental counterpart of Section 3.3. Most noticeably, the simulations exhibit a local minimum moving with alignments for angles larger than 20° where measurements keep any feature around 40 eV. This discrepancy can be explained by the absence of the Cooper-like minimum in the OCS effective molecular

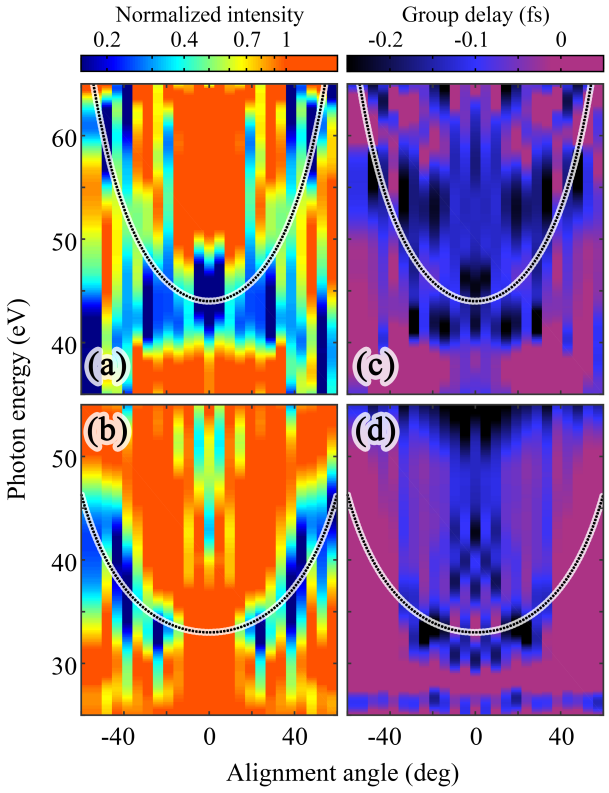

Figure 7: TDDFT simulations of HHS intensities (left panels) and group delays (right) in CO_2 (top) and OCS (bottom). Colormaps show the normalized harmonic yield of Eq. (11) and group delay of Eq. (13) as functions of molecular alignment with respect to the laser polarization ($\theta = 0$ for parallel alignment). The short-trajectory signal is extracted using the APT ionization-seed procedure described in Section 4.2.1. In each panel, the parabolic solid curve labels the empirical energy of the two-center interference as given by Eq. (10) with $\beta = 1$ for CO_2 and $\beta = 0.7$ for OCS. Further details about the computation and comparison to their experimental counterparts can be found in [25]. Reproduced from [36], with the permission of AIP Publishing.

potentials. Indeed, precise description of the location of a Cooper minimum is hard to achieve and requires a very accurate description of the continuum wave function [36, 99] which goes beyond the capabilities of the LDA functional and effective atomic potentials used here.

Finally, the numerical group delays for both CO_2 and OCS in Panels (c) and (d) generally do not exhibit clear patterns that can be compared to their associated spectral intensity or measurements. These discrepancies underline the effort that is still needed, *e.g.*, in terms of fine-tuning the APT seeding and signal post-processing, to extract meaningful spectral phase information out of TDDFT HHS simulations.

4.3. Sub-cycle molecular high-harmonic spectroscopy

For comparison with experiments, the OCS simulations of Fig. 7 have limited relevance because they lack an essential Cooper-like feature, as discussed in the previous section. Taken on their own, however, these results shed very interesting light on how sub-laser-cycle processes can shape HHS signals. Ultimately observing charge migration with HHS will require sub-cycle resolution when processing harmonics spectral amplitudes and phases.

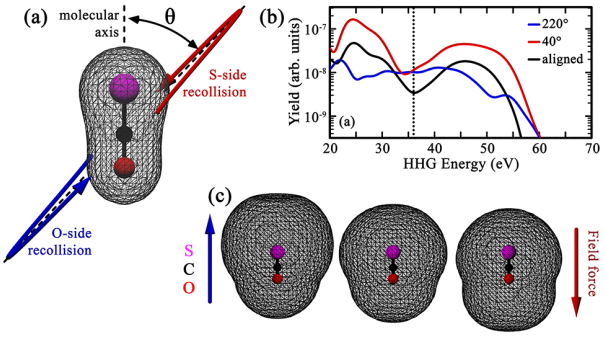

Figure 8: Illustration of sub-cycle HHS in OCS. Panel (a) sketches the differences for recollisions from the S and O sides of the molecule, with their respective spectral intensity shown in Panel (b). Panel (c) shows the redistribution of the electronic density imposed by a static electric field. More details about the simulations and analyses can be found in [25]; licensed under a Creative Commons Attribution (CC BY) license.

The OCS molecule does not possess full inversion symmetry, which means that harmonic emission from successive half laser-cycles or opposite orientations (angle θ and $\theta + \pi$) is associated with recollisions from opposite sides of the target, as illustrated in Fig. 8 (a). For oriented samples, and without the half-laser-cycle resolution, the separation of the signals from the two orientations is less straightforward and involves both odd and even harmonic orders [100]. In single-molecule simulations, which naturally define an oriented target, the selection of a single half-cycle short-trajectory harmonic signal is achieved by combining the APT ionization seed with recollision-time windowing, as discussed in Section 4.2.1. Fig. 8 (b) compares the HHS intensity stemming from recollision from opposite sides of the OCS molecule, each yielding markedly different results: recollision from the S side (red curve) gives a clear two-center interference minimum centered slightly below 45 eV, whereas recollision from the O side (blue curve) does not yield any sign of a two-center interference. Note that in the aligned signal, because the two orientations are added coherently and can therefore interfere, the two-center minimum is shifted to a slightly higher energy (see vertical dashed line) [25, 74].

In the context of the QRS factorization of Eq. (1), the qualitative difference in the HHS results between the two orientations might at first seem surprising. Indeed, the continuum wave function ψ_c in the field-free RDME definition (2) only changes sign between opposite angles, such that $\sigma(\nu;\theta) = \sigma(\nu;\theta+\pi)$ and thus

$$\left|\frac{HHG(\nu;\theta)}{HHG(\nu;\theta+\pi)}\right| = \sqrt{\frac{\Gamma(\theta)}{\Gamma(\theta+\pi)}},$$

ruling out harmonic-energy-dependent differences between the two results. Instead, the difference stems from sub-cycle polarization effects in the molecule's bound density, which alters the distribution of electrons in OCS between opposite recollision orientations, as illustrated in Fig. 8 (c). Without a driving field, the distribution of charges in OCS is naturally biased towards the S end of the molecule (middle panels). This imbalance is further exacerbated or reduced when the driving laser force points O-to-S or the opposite direction (see side panels and associated arrows). When including this sub-cycle polarization effects in the two-center RDME decomposition, Eq. (7), harmonics associated with recollision from the S side experience more balanced centers, which is conducive to the interference minimum observed in the associated spectral intensity. On the other hand, recollisions from the O side are when the two centers of density are most imbalanced, therefore erasing the interference minimum. Finally, the strength of such sub-cycle polarization effects depends on the projection of the electric field onto the molecular axis [81], which in turn can explain why two-center interference minima are only observed for some angles in Fig. 7 (b). More details about the orientation-dependent and sub-cycle HHS analyses can be found in [25].

The OCS results of Fig. 7 are both a cautionary example and promising outlook for charge migration studies with HHS. On the one hand, they clearly illustrate how the reshaping of the target's electronic structure, here due to the driving laser field, can in turn drastically reshape harmonic spectral properties. Conversely, it means that target-specific spectral signals may not be field free [101] and similar polarization effects can possibly influence or overwrite migration dynamics of interest in the compound. At leading order, it seems that orienting linear molecules orthogonal to the laser polarization yields a quasi-field free HHS configuration [25, 81]; generalization to more complex targets, however, is not straightforward. On the other hand, seeing the polarization-driven redistribution of charge within the molecule as a transient two-center interference effect clearly demonstrates the potential of HHS to resolving time-dependent sub-cycle migration dynamics.

5. Outlook

In this review, we have focused on the spectroscopic part of molecular HHS, namely how one can extract a signal that can be uniquely related to a target's electronic structure. The success of this extraction hinges upon the simultaneous recording of multidimensional signals, including both the target-specific spectral amplitude and phase. In most cases, molecular-frame resolution with control of the targets' alignment or orientation is also required, as exemplified by the OCS studies discussed in Sections 3.3 and 4.3. Charge migration studies however add to the complexity of these measurements by requiring one of these dimensions to be clearly tied to time, with attosecond resolution.

Because of the complex requirements of HHS experiments, ideal near-term targets for extending HHS measurements to charge migration may be unique to one's experimental capabilities. In general, however, a good candidate should (i) be able to trigger and sustain charge migration, (ii) have well-calibrated reference feature(s) against which migration-induced signals can be identified, and (iii) have experimentally-accessible dimensions that are sensitive and directly related to the charge migration dynamics. In the longer term, achieving a versatile application of HHS for charge migration studies will also require a more comprehensive approach including (i) understanding the migrating dynamics itself, and how it is regulated by the target's chemical properties, and (ii) selectively triggering a well-identified migration mode at the initial ionization step. We thus briefly discuss perspectives for these questions in Sections 5.1-5.3 with the exception of well-calibrated reference features which were previously discussed in Sections 3 and 4.

5.1. Temporal dimension

Harmonic generation possesses a natural sub-femtosecond time scale associated with the ionization-to-recollision delay [45, 46]. Accessing this temporal dimension for charge migration studies, nonetheless, requires deliberate efforts. Most directly, the ionization-to-recollision delay can be controlled by tuning the mid-IR-laser wavelength. Experimentally, the nanometer-scale (meV) wavelength-tuning precision required to resolve attosecond dynamics can be obtained with optical parametric amplification – see the experimental apparatus discussion of Section 2.1. However, note that the deconvolution of the temporal dimension in HHS with a continuous wavelength scan is not entirely straightforward as both the ionization and recollision times are affected with changing the driving laser period.

Borrowing from the attosecond-pulse-train seed of Section 4.2.1, the synchronization of a XUV ionization pulse with the mid-IR driving field would provide a more direct temporal dimension. Assuming the XUV pulse is responsible for triggering the migrating dynamics, its delay with respect to a sub-cycle of the mid-IR corresponds directly to the time axis. Obviously this method involves steep experimental challenges. For instance, the power required to produce an XUV pulse and a mid-IR driving field at HHG intensities is significantly greater than in a traditional HHS experiment. Similarly, the experiment would exhibit the challenges faced in streaking [11, 102] as the freed electron would have a non-zero kinetic energy upon ionization, in contrast to HHG [85], and these non-zero initial velocities will impact acceleration dynamics in the continuum. Finally, the XUV pulse must have a sub-femtosecond duration in order to set a precise migration start time which requires a large energetic bandwith opening the possibility for multiple ionization channels. Alternative to HHS, XUV-initialized migration dynamics might be more readily observable in ionization spectroscopy [90, 103, 104, 105, 106].

5.2. Migrating dynamics

As discussed in Sections 3.3 and 4.3, signatures of charge migration dynamics will likely be convoluted in HHS signals. Therefore, some knowledge or understanding of the

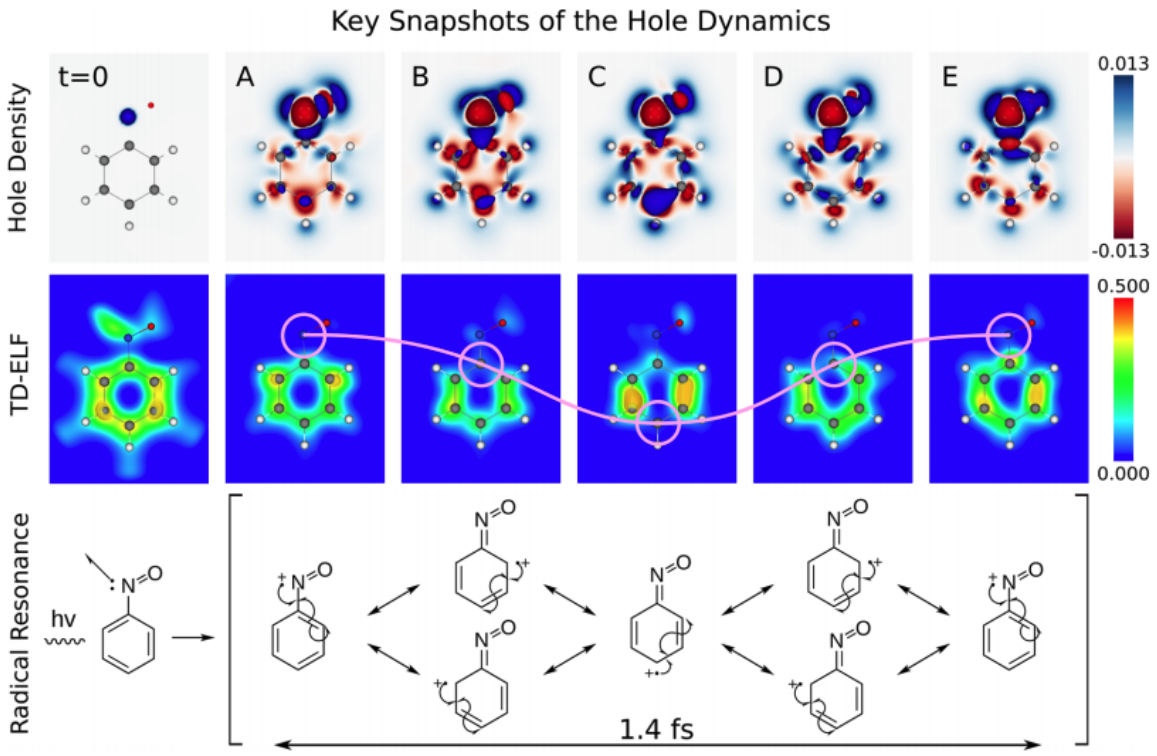

Figure 9: Snapshots of the hole migration in nitrosobenzene at five time delays (A-E) from ionization represented in three different ways. The (top) row shows the hole density evolution. The (middle) row shows the TDELF with magenta circles indicating regions of decreased electron localization. The (bottom) row shows a qualitative mapping onto the Lewis dot resonant structures using the "electron pushing" mechanism. More details on these simulations can be found at [107]. Not subject to U.S. Copyright.

migration itself would greatly enhance perspectives for unambiguous deconvolution and access to the dynamics in experimental data. Charge migration dynamics, however, involve many correlated electrons in ways that can be hard to predict, but, fortuitously, theory has the unique advantage that it can look at the charge migration dynamics directly, in real time and real space, without practical limitations of initializing and probing it with experimentally accessible means. As such, input from high-performance calculations continue to play an important role in understanding measurements and also guiding experimental design.

Fig. 9 illustrates the insights gained from theory by viewing the migration of charge in nitrosobenzene in several complementary ways [107]. Here the evolution of an electron hole is computed with TDDFT, following a core level ionization from the nitrogen K-edge. The top row shows the time-dependent evolution of the hole density around the molecule. The middle panel shows the time-dependent electron localization function (TDELF) [108, 109] which highlights the transience of specific chemical structures in the molecules such as lone pairs, bonds, holes. Finally, the bottom panel presents a mechanistic description of the migration dynamics in terms of “electron pushing” in the Lewis dot structures [110].

5.3. Initiating migration

Not all ionization excitations lead to a migration of charge, which makes the initial ionization step as important as the migration motion itself. Conceptually, it is easiest to imagine creating a localized hole as the best way to trigger a subsequent migration [21, 111]. A favorable method for generating a localized hole is through single photon core level ionization [24]; however, this is not possible using mid-IR lasers. Luckily, localized valence-shell ionization can be achieved using a mid-IR driving field in certain molecules, with control provided through molecular alignment or orientation [81].

Interestingly, ionization spectroscopy in the halomethane family has demonstrated that one can also chemically control hole localization in valence-shell ionization by changing the halogen functionalization [112]. This study also exemplifies the importance of comparing spectroscopic measurements across families of targets, *e.g.*, with functionalization being one of the dimensions in HHS. Note that ionization inducing a migration of charge does not necessarily necessitate the creation of a spatially localized hole. For instance, it has been shown that benzene can exhibit a long lasting migration that follows a breathing motion of electron density in and out of the carbon ring [113].

6. Summary

In this article, we presented an overview of progress towards characterizing charge migration through high-harmonic spectroscopy which presents itself as an ideal technique due to its inherent attosecond time resolution. We first began with a quantitative analysis of the emitted harmonic radiation and outlined a method to isolate the structural contributions of the ion, known as the RDME, in both the amplitude and phase of the harmonic spectrum. Using this method, we examined two structural features, two-center interferences and Cooper minima, in small molecules using HHS. At first, we presented studies of CO_2 and CH_3Cl where only one feature is present. We then explored OCS, which has both features, to illustrate the crucial importance of multidimensional analysis to deconvolve each feature's contributions to the emitted radiation. This will be crucial to isolating time-dependent contributions associated with charge migration.

As HHS characterization of charge migration requires both an experimental and theoretical effort, we outlined two simulation methods with their respective strengths and shortcomings in comparison to measurements: (i) a semi-classical approach based on three-step factorization, and (ii) a direct numerical approach based on first principles calculations. Within the direct approach, a method for isolating the short-trajectories of HHG was introduced, and illustrated by comparison to experimental results, and allowed for a further examination of sub-cycle molecular HHS. This sub-cycle resolution revealed the impact of the driving field on electron dynamics and hence provided insight on future experimental design.

Throughout the experimental and theoretical discussions, we purposefully examined features, such as two-center interferences and Cooper minima, in our overview of HHS analysis techniques because these features are structural, *i.e.* caused by the ion's charge density distribution. Hence, the time-independent characterizations of these features will act as key references for charge migration studies where the charge density will gain a time-dependence and transiently vary these previously static features in the phase and amplitude of the emitted harmonic radiation.

Finally, we considered the introduction of a controllable temporal dimension to HHS and commented on the need for additional theoretical computations of migratory dynamics, the chemical properties which impact them, and experimental/theoretical ionization spectroscopy for control over the triggering of specific migration modes. Overall, continuing efforts to induce, control, and observe molecular charge migration hold both significant promise and challenges.

7. Declaration of Competing Interests

The authors declare that they have no known competing financial interests or personal relationships that could have appeared to influence the work reported in this paper.

8. Acknowledgements

This work was supported by the US Department of Energy, Office of Science, Office of Basic Energy Sciences, under Award No. DE-SC0012462.

References

[1] L.S. Cederbaum and J. Zobeley. Ultrafast charge migration by electron correlation. Chemical Physics Letters, 307(3):205 – 210, 1999. ISSN 0009-2614. doi: https://doi.org/10.1016/S0009-2614(99)00508-4. URL http://www.sciencedirect.com/science/article/pii/S0009261499005084.

[2] S. N. Pisharody and R. R. Jones. Probing two-electron dynamics of an atom. Science, 303(5659):813–815, 2004. ISSN 0036-8075. doi: 10.1126/science.1092220. URL https://science.sciencemag.org/content/303/5659/813.

[3] J. Feist, S. Nagele, R. Pazourek, E. Persson, B. I. Schneider, L. A. Collins, and J. Burgdörfer. Probing electron correlation via attosecond xuv pulses in the two-photon double ionization of helium. Phys. Rev. Lett., 103:063002, Aug 2009. doi: 10.1103/PhysRevLett.103.063002. URL https://link.aps.org/doi/10.1103/PhysRevLett.103.063002.

[4] J. Breidbach and L. S. Cederbaum. Universal attosecond response to the removal of an electron. Phys. Rev. Lett., 94:033901, Jan 2005. doi: 10.1103/PhysRevLett.94.033901. URL https://link.aps.org/doi/10.1103/PhysRevLett.94.033901.

[5] F. Remacle and R. D. Levine. An electronic time scale in chemistry. Proceedings of the National Academy of Sciences, 103(18):6793–6798, 2006. doi: 10.1073/pnas.0601855103. URL https://www.pnas.org/content/103/18/6793.

[6] Franck Lépine, Misha Y. Ivanov, and Marc J. J. Vrakking. Attosecond molecular dynamics: fact or fiction? Nature Photonics, 8(3):195–204, 2014. ISSN 1749-4893. doi: 10.1038/nphoton.2014.25. URL https://doi.org/10.1038/nphoton.2014.25.

[7] Matthias F. Kling, Philipp von den Hoff, Irina Znakovskaya, and Regina de Vivie-Riedle. (sub-)femtosecond control of molecular reactions via tailoring the electric field of light. Phys. Chem. Chem. Phys., 15:9448–9467, 2013. doi: 10.1039/C3CP50591J. URL http://dx.doi.org/10.1039/C3CP50591J.

[8] J. Breidbach and L. S. Cederbaum. Migration of holes: Formalism, mechanisms, and illustrative applications. The Journal of Chemical Physics, 118(9):3983–3996, 2003. doi: 10.1063/1.1540618. URL https://doi.org/10.1063/1.1540618.

[9] André D. Bandrauk, Stephane Chelkowski, and Hong Shon Nguyen. Attosecond localization of electrons in molecules. International Journal of Quantum Chemistry, 100(6):834–844, 2004. doi: 10.1002/qua.20252. URL https://onlinelibrary.wiley.com/doi/abs/10.1002/qua.20252.

[10] Holger Hennig, Jörg Breidbach, and Lorenz S. Cederbaum. Electron correlation as the driving force for charge transfer: Charge migration following ionization in n-methyl acetamide. The Journal of Physical Chemistry A, 109(3):409–414, 2005. doi: 10.1021/jp046232s. URL https://doi.org/10.1021/jp046232s. PMID: 16833360.

[11] M. Drescher, M. Hentschel, R. Kienberger, M. Uiberacker, V. Yakovlev, A. Scrinzi, Th Westerwalbesloh, U. Kleineberg, U. Heinzmann, and F. Krausz. Time-resolved atomic inner-shell spectroscopy. Nature, 419(6909):803–807, 2002. ISSN 1476-4687. doi: 10.1038/nature01143. URL https://doi.org/10.1038/nature01143.

[12] M. Uiberacker, Th Uphues, M. Schultze, A. J. Verhoef, V. Yakovlev, M. F. Kling, J. Rauschenberger, N. M. Kabachnik, H. Schröder, M. Lezius, K. L. Kompa, H.-G. Muller, M. J. J. Vrakking, S. Hendel, U. Kleineberg, U. Heinzmann, M. Drescher, and F. Krausz. Attosecond real-time observation of electron tunnelling in atoms. Nature, 446(7136):627–632, 2007. ISSN 1476-4687. doi: 10.1038/nature05648. URL https://doi.org/10.1038/nature05648.

[13] M. Schultze, M. Fieß, N. Karpowicz, J. Gagnon, M. Korbman,

M. Hofstetter, S. Neppl, A. L. Cavalieri, Y. Komninos, Th. Mercouris, C. A. Nicolaides, R. Pazourek, S. Nagele, J. Feist, J. Burgdörfer, A. M. Azzeer, R. Ernstorfer, R. Kienberger, U. Kleineberg, E. Goulielmakis, F. Krausz, and V. S. Yakovlev. Delay in photoemission. Science, 328(5986):1658–1662, 2010. ISSN 0036-8075. doi: 10.1126/science.1189401. URL https://science.sciencemag.org/content/328/5986/1658.

[14] K. Klünder, J. M. Dahlström, M. Gisselbrecht, T. Fordell, M. Swoboda, D. Guénot, P. Johnsson, J. Caillat, J. Mauritsson, A. Maquet, R. Taïeb, and A. L'Huillier. Probing single-photon ionization on the attosecond time scale. Phys. Rev. Lett., 106:143002, Apr 2011. doi: 10.1103/PhysRevLett.106.143002. URL https://link.aps.org/doi/10.1103/PhysRevLett.106.143002.

[15] G. Sansone, F. Kelkensberg, J. F. Pérez-Torres, F. Morales, M. F. Kling, W. Siu, O. Ghafur, P. Johnsson, M. Swoboda, E. Benedetti, F. Ferrari, F. Lépine, J. L. Sanz-Vicario, S. Zherebtsov, I. Znakovskaya, A. L'Huillier, M. Yu Ivanov, M. Nisoli, F. Martín, and M. J. J. Vrakking. Electron localization following attosecond molecular photoionization. Nature, 465(7299):763–766, 2010. doi: 10.1038/nature09084. URL https://doi.org/10.1038/nature09084.

[16] F. Kelkensberg, W. Siu, J. F. Pérez-Torres, F. Morales, G. Gademann, A. Rouzée, P. Johnsson, M. Lucchini, F. Calegari, J. L. Sanz-Vicario, F. Martín, and M. J. J. Vrakking. Attosecond control in photoionization of hydrogen molecules. Phys. Rev. Lett., 107: 043002, Jul 2011. doi: 10.1103/PhysRevLett.107.043002. URL https://link.aps.org/doi/10.1103/PhysRevLett.107.043002.

[17] W. Siu, F. Kelkensberg, G. Gademann, A. Rouzée, P. Johnsson, D. Dowek, M. Lucchini, F. Calegari, U. De Giovannini, A. Rubio, R. R. Lucchese, H. Kono, F. Lépine, and M. J. J. Vrakking. Attosecond control of dissociative ionization of o_2 molecules. Phys. Rev. A, 84:063412, Dec 2011. doi: 10.1103/PhysRevA.84.063412. URL https://link.aps.org/doi/10.1103/PhysRevA.84.063412.

[18] Olga Smirnova, Yann Mairesse, Serguei Patchkovskii, Nirit Dudovich, David Villeneuve, Paul Corkum, and Misha Yu Ivanov. High harmonic interferometry of multi-electron dynamics in molecules. Nature, 460(7258):972–977, 2009. ISSN 1476-4687. doi: 10.1038/nature08253. URL https://doi.org/10.1038/nature08253.

[19] Y. Mairesse, J. Higuet, N. Dudovich, D. Shafir, B. Fabre, E. Mével, E. Constant, S. Patchkovskii, Z. Walters, M. Yu. Ivanov, and O. Smirnova. High harmonic spectroscopy of multichannel dynamics in strong-field ionization. Phys. Rev. Lett., 104:213601, May 2010. doi: 10.1103/PhysRevLett.104.213601. URL https://link.aps.org/doi/10.1103/PhysRevLett.104.213601.

[20] F. Calegari, D. Ayuso, A. Trabattoni, L. Belshaw, S. De Camillis, S. Anumula, F. Frassetto, L. Poletto, A. Palacios, P. Decleva, J. B. Greenwood, F. Martín, and M. Nisoli. Ultrafast electron dynamics in phenylalanine initiated by attosecond pulses. Science, 346(6207): 336–339, 2014. ISSN 0036-8075. doi: 10.1126/science.1254061. URL https://science.sciencemag.org/content/346/6207/336.

[21] P. M. Kraus, B. Mignolet, D. Baykusheva, A. Rupenyan, L. Horný, E. F. Penka, G. Grassi, O. I. Tolstikhin, J. Schneider, F. Jensen, L. B. Madsen, A. D. Bandrauk, F. Remacle, and H. J. Wörner. Measurement and laser control of attosecond charge migration in ionized iodoacetylene. Science, 350(6262):790–795, 2015. ISSN 0036-8075. doi: 10.1126/science.aab2160. URL https://science.sciencemag.org/content/350/6262/790.

[22] A. Trabattoni, M. Galli, M. Lara-Astiaso, A. Palacios, J. Greenwood, I. Tavernelli, P. Decleva, M. Nisoli, F. Martín, and F. Calegari. Charge migration in photo-ionized aromatic amino acids. Philosophical Transactions of the Royal Society A, 377(2145), 2019. ISSN 1471-2962. doi: 10.1098/rsta.2017.0472. URL https://royalsocietypublishing.org/doi/10.1098/rsta.2017.0472.

[23] Manuel Lara-Astiaso, Alicia Palacios, Piero Decleva, Ivano Tavernelli, and Fernando Martín. Role of electron-nuclear coupled dynamics on charge migration induced by attosecond pulses in glycine. Chemical Physics Letters, 683:357 – 364, 2017. ISSN 0009-2614. doi: https://doi.org/10.1016/j.cplett.2017.05.008. URL http://www.sciencedirect.com/science/article/pii/S0009261417304359. Ahmed Zewail (1946-2016) Commemoration Issue of Chemical Physics Letters.

[24] Alexander I. Kuleff, Nikolai V. Kryzhevoi, Markus Pernpointner, and Lorenz S. Cederbaum. Core ionization initiates subfemtosecond charge migration in the valence shell of molecules. Phys. Rev. Lett., 117:093002, Aug 2016. doi: 10.1103/PhysRevLett.117.093002. URL https://link.aps.org/doi/10.1103/PhysRevLett.117.093002.

[25] François Mauger, Paul M. Abanador, Timothy D. Scarborough, Timothy T. Gorman, Pierre Agostini, Louis F. DiMauro, Kenneth Lopata, Kenneth J. Schafer, and Mette B. Gaarde. High-harmonic spectroscopy of transient two-center interference calculated with time-dependent density-functional theory. Structural Dynamics, 6 (4):044101, 2019. doi: 10.1063/1.5111349. URL https://doi.org/10.1063/1.5111349.

[26] J. P. Marangos. The measurement of ultrafast electronic and structural dynamics with x-rays. Philosophical transactions. Series A, Mathematical, physical, and engineering sciences, 377(2145): 20170481–20170481, May 2019. ISSN 1471-2962. doi: 10.1098/rsta.2017.0481. URL https://pubmed.ncbi.nlm.nih.gov/30929630.30929630[pmid].

[27] Philippe Antoine, Anne L'Huillier, and Maciej Lewenstein. Attosecond pulse trains using high–order harmonics. Phys. Rev. Lett., 77: 1234–1237, Aug 1996. doi: 10.1103/PhysRevLett.77.1234. URL https://link.aps.org/doi/10.1103/PhysRevLett.77.1234.

[28] M. B. Gaarde, F. Salin, E. Constant, Ph. Balcou, K. J. Schafer, K. C. Kulander, and A. L'Huillier. Spatiotemporal separation of high harmonic radiation into two quantum path components. Phys. Rev. A, 59:1367–1373, Feb 1999. doi: 10.1103/PhysRevA.59.1367. URL https://link.aps.org/doi/10.1103/PhysRevA.59.1367.

[29] Enikö Seres, József Seres, Ferenc Krausz, and Christian Spielmann. Generation of coherent soft-x-ray radiation extending far beyond the titanium *l* edge. Phys. Rev. Lett., 92:163002, Apr 2004. doi: 10.1103/PhysRevLett.92.163002. URL https://link.aps.org/doi/10.1103/PhysRevLett.92.163002.

[30] Manfred Lein. Attosecond probing of vibrational dynamics with high-harmonic generation. Phys. Rev. Lett., 94:053004, Feb 2005. doi: 10.1103/PhysRevLett.94.053004. URL https://link.aps.org/doi/10.1103/PhysRevLett.94.053004.

[31] S. Baker, J. S. Robinson, C. A. Haworth, H. Teng, R. A. Smith, C. C. Chirilă, M. Lein, J. W. G. Tisch, and J. P. Marangos. Probing proton dynamics in molecules on an attosecond time scale. Science, 312(5772):424–427, 2006. ISSN 0036-8075. doi: 10.1126/science.1123904. URL https://science.sciencemag.org/content/312/5772/424.

[32] Xibin Zhou, Robynne Lock, Wen Li, Nick Wagner, Margaret M. Murnane, and Henry C. Kapteyn. Molecular recollision interferometry in high harmonic generation. Phys. Rev. Lett., 100:073902, Feb 2008. doi: 10.1103/PhysRevLett.100.073902. URL https://link.aps.org/doi/10.1103/PhysRevLett.100.073902.

[33] Hans Jakob Wörner, Hiromichi Niikura, Julien B. Bertrand, P. B. Corkum, and D. M. Villeneuve. Observation of electronic structure minima in high-harmonic generation. Phys. Rev. Lett., 102:103901, Mar 2009. doi: 10.1103/PhysRevLett.102.103901. URL https://link.aps.org/doi/10.1103/PhysRevLett.102.103901.

[34] Anh-Thu Le, R. R. Lucchese, M. T. Lee, and C. D. Lin. Probing molecular frame photoionization via laser generated high-order harmonics from aligned molecules. Phys. Rev. Lett., 102:203001, May 2009. doi: 10.1103/PhysRevLett.102.203001. URL https://link.aps.org/doi/10.1103/PhysRevLett.102.203001.

[35] Timothy D. Scarborough, Timothy T. Gorman, François Mauger, Péter Sándor, Sanjay Khatri, Mette B. Gaarde, Kenneth J. Schafer, Pierre Agostini, and Louis F. DiMauro. Full characterization of a molecular cooper minimum using high-harmonic spectroscopy. Applied Sciences, 8(7), 2018. ISSN 2076-3417. doi: 10.3390/app8071129. URL https://www.mdpi.com/2076-3417/8/7/1129.

[36] T. T. Gorman, T. D. Scarborough, P. M. Abanador, F. Mauger, D. Kiesewetter, P. Sándor, S. Khatri, K. Lopata, K. J. Schafer, P. Agostini, M. B. Gaarde, and L. F. DiMauro. Probing the inter-

play between geometric and electronic-structure features via high-harmonic spectroscopy. The Journal of Chemical Physics, 150(18): 184308, 2019. doi: 10.1063/1.5086036. URL https://doi.org/10.1063/1.5086036.

[37] J. Itatani, J. Levesque, D. Zeidler, Hiromichi Niikura, H. Pépin, J. C. Kieffer, P. B. Corkum, and D. M. Villeneuve. Tomographic imaging of molecular orbitals. Nature, 432(7019):867–871, 2004. ISSN 1476-4687. URL https://doi.org/10.1038/nature03183.

[38] Serguei Patchkovskii, Zengxiu Zhao, Thomas Brabec, and D. M. Villeneuve. High harmonic generation and molecular orbital tomography in multielectron systems: Beyond the single active electron approximation. Phys. Rev. Lett., 97:123003, Sep 2006. doi: 10.1103/PhysRevLett.97.123003. URL https://link.aps.org/doi/10.1103/PhysRevLett.97.123003.

[39] S. Haessler, J. Caillat, W. Boutu, C. Giovanetti-Teixeira, T. Ruchon, T. Auguste, Z. Diveki, P. Breger, A. Maquet, B. Carré, R. Taïeb, and P. Salières. Attosecond imaging of molecular electronic wavepackets. Nature Physics, 6(3):200–206, 2010. ISSN 1745-2481. doi: 10.1038/nphys1511. URL https://doi.org/10.1038/nphys1511.

[40] C. Vozzi, M. Negro, F. Calegari, G. Sansone, M. Nisoli, S. De Silvestri, and S. Stagira. Generalized molecular orbital tomography. Nature Physics, 7(10):822–826, 2011. ISSN 1745-2481. doi: 10.1038/nphys2029. URL https://doi.org/10.1038/nphys2029.

[41] X. F. Li, A. L'Huillier, M. Ferray, L. A. Lompré, and G. Mainfray. Multiple-harmonic generation in rare gases at high laser intensity. Phys. Rev. A, 39:5751–5761, Jun 1989. doi: 10.1103/PhysRevA.39.5751. URL https://link.aps.org/doi/10.1103/PhysRevA.39.5751.

[42] Anne L'Huillier and Ph. Balcou. High-order harmonic generation in rare gases with a 1-ps 1053-nm laser. Phys. Rev. Lett., 70:774–777, Feb 1993. doi: 10.1103/PhysRevLett.70.774. URL https://link.aps.org/doi/10.1103/PhysRevLett.70.774.

[43] K. J. Schafer, Baorui Yang, L. F. DiMauro, and K. C. Kulander. Above threshold ionization beyond the high harmonic cutoff. Phys. Rev. Lett., 70:1599–1602, Mar 1993. doi: 10.1103/PhysRevLett.70.1599. URL https://link.aps.org/doi/10.1103/PhysRevLett.70.1599.

[44] P. B. Corkum. Plasma perspective on strong field multiphoton ionization. Phys. Rev. Lett., 71:1994–1997, Sep 1993. doi: 10.1103/PhysRevLett.71.1994. URL https://link.aps.org/doi/10.1103/PhysRevLett.71.1994.

[45] M. Lewenstein, Ph. Balcou, M. Yu. Ivanov, Anne L'Huillier, and P. B. Corkum. Theory of high-harmonic generation by low-frequency laser fields. Phys. Rev. A, 49:2117–2132, Mar 1994. doi: 10.1103/PhysRevA.49.2117. URL https://link.aps.org/doi/10.1103/PhysRevA.49.2117.

[46] P. Salières, B. Carré, L. Le Déroff, F. Grasbon, G. G. Paulus, H. Walther, R. Kopold, W. Becker, D. B. Milošević, A. Sanpera, and M. Lewenstein. Feynman's path-integral approach for intense-laser-atom interactions. Science, 292(5518):902–905, 2001. ISSN 0036-8075. doi: 10.1126/science.108836. URL https://science.sciencemag.org/content/292/5518/902.

[47] M. Lein, N. Hay, R. Velotta, J. P. Marangos, and P. L. Knight. Interference effects in high-order harmonic generation with molecules. Phys. Rev. A, 66:023805, Aug 2002. doi: 10.1103/PhysRevA.66.023805. URL https://link.aps.org/doi/10.1103/PhysRevA.66.023805.

[48] C. Vozzi, F. Calegari, E. Benedetti, J.-P. Caumes, G. Sansone, S. Stagira, M. Nisoli, R. Torres, E. Heesel, N. Kajumba, J. P. Marangos, C. Altucci, and R. Velotta. Controlling two-center interference in molecular high harmonic generation. Phys. Rev. Lett., 95: 153902, Oct 2005. doi: 10.1103/PhysRevLett.95.153902. URL https://link.aps.org/doi/10.1103/PhysRevLett.95.153902.

[49] Tsuneto Kanai, Shinichirou Minemoto, and Hirofumi Sakai. Quantum interference during high-order harmonic generation from aligned molecules. Nature, 435(7041):470–474, 2005. ISSN 1476-4687. doi: 10.1038/nature03577. URL https://doi.org/10.1038/nature03577.

[50] W. Boutu, S. Haessler, H. Merdji, P. Breger, G. Waters, M. Stankiewicz, L. J. Frasinski, R. Taieb, J. Caillat, A. Maquet, P. Monchicourt, B. Carre, and P. Salieres. Coherent control of attosecond emission from aligned molecules. Nature Physics, 4(7): 545–549, 2008. ISSN 1745-2481. doi: 10.1038/nphys964. URL https://doi.org/10.1038/nphys964.

[51] H. J. Wörner, J. B. Bertrand, P. Hockett, P. B. Corkum, and D. M. Villeneuve. Controlling the interference of multiple molecular orbitals in high-harmonic generation. Phys. Rev. Lett., 104:233904, Jun 2010. doi: 10.1103/PhysRevLett.104.233904. URL https://link.aps.org/doi/10.1103/PhysRevLett.104.233904.

[52] A. Rupenyan, P. M. Kraus, J. Schneider, and H. J. Wörner. Quantum interference and multielectron effects in high-harmonic spectra of polar molecules. Phys. Rev. A, 87:031401, Mar 2013. doi: 10.1103/PhysRevA.87.031401. URL https://link.aps.org/doi/10.1103/PhysRevA.87.031401.

[53] Marie Labeye, Fran çois Risoud, Camille Lévêque, Jérémie Caillat, Alfred Maquet, Tahir Shaaran, Pascal Salières, and Richard Taïeb. Dynamical distortions of structural signatures in molecular high-order harmonic spectroscopy. Phys. Rev. A, 99:013412, Jan 2019. doi: 10.1103/PhysRevA.99.013412. URL https://link.aps.org/doi/10.1103/PhysRevA.99.013412.

[54] John W. Cooper. Photoionization from outer atomic subshells. a model study. Phys. Rev., 128:681–693, Oct 1962. doi: 10.1103/PhysRev.128.681. URL https://link.aps.org/doi/10.1103/PhysRev.128.681.

[55] R. W. Ditchburn, J. Tunstead, and J. G. Yates. The Continuous Absorption of Light in Potassium Vapour. Proceedings of the Royal Society of London Series A, 181:386–399, July 1943. doi: 10.1098/rspa.1943.0016.

[56] T. A. Carlson, M. O. Krause, W. A. Svensson, P. Gerard, F. A. Grimm, T. A. Whitley, and B. P. Pullen. Photoelectron dynamics of the cooper minimum in free molecules. Zeitschrift für Physik D Atoms, Molecules and Clusters, 2(4):309–318, Dec 1986. ISSN 1431-5866. doi: 10.1007/BF01426235. URL https://doi.org/10.1007/BF01426235.

[57] I. Novak, J.M. Benson, and A.W. Potts. Uv angle resolved photoelectron spectra of fluoro and chloromethane using synchrotron radiation. Journal of Electron Spectroscopy and Related Phenomena, 41(2):225 – 233, 1986. ISSN 0368-2048. doi: https://doi.org/10.1016/0368-2048(86)85005-8. URL http://www.sciencedirect.com/science/article/pii/0368204886850058.

[58] D.M.P. Holland, I. Powis, G. Öhrwall, L. Karlsson, and W. von Niessen. A study of the photoionisation dynamics of chloromethane and iodomethane. Chemical Physics, 326(2):535 – 550, 2006. ISSN 0301-0104. doi: https://doi.org/10.1016/j.chemphys.2006.03.017. URL http://www.sciencedirect.com/science/article/pii/S0301010406001595.

[59] Henrik Stapelfeldt and Tamar Seideman. Colloquium: Aligning molecules with strong laser pulses. Rev. Mod. Phys., 75:543–557, Apr 2003. doi: 10.1103/RevModPhys.75.543. URL https://link.aps.org/doi/10.1103/RevModPhys.75.543.

[60] Bing Shan and Zenghu Chang. Dramatic extension of the high-order harmonic cutoff by using a long-wavelength driving field. Phys. Rev. A, 65:011804, Dec 2001. doi: 10.1103/PhysRevA.65.011804. URL https://link.aps.org/doi/10.1103/PhysRevA.65.011804.

[61] P. Colosimo, G. Doumy, C. I. Blaga, J. Wheeler, C. Hauri, F. Catoire, J. Tate, R. Chirla, A. M. March, G. G. Paulus, H. G. Muller, P. Agostini, and L. F. DiMauro. Scaling strong-field interactions towards the classical limit. Nature Physics, 4(5):386–389, 2008. ISSN 1745-2481. doi: 10.1038/nphys914. URL https://doi.org/10.1038/nphys914.

[62] P. M. Paul, E. S. Toma, P. Breger, G. Mullot, F. Augé, Ph. Balcou, H. G. Muller, and P. Agostini. Observation of a train of attosecond pulses from high harmonic generation. Science, 292(5522):1689–1692, 2001. ISSN 0036-8075. doi: 10.1126/science.1059413. URL https://science.sciencemag.org/content/292/5522/1689.

[63] H.G. Muller. Reconstruction of attosecond harmonic beating by interference of two-photon transitions. Applied Physics B, 74(1): s17–s21, Jun 2002. doi: 10.1007/s00340-002-0894-8. URL https:

//doi.org/10.1007/s00340-002-0894-8.

[64] Anh-Thu Le, R. R. Lucchese, S. Tonzani, T. Morishita, and C. D. Lin. Quantitative rescattering theory for high-order harmonic generation from molecules. Phys. Rev. A, 80:013401, Jul 2009. doi: 10.1103/PhysRevA.80.013401. URL https://link.aps.org/doi/10.1103/PhysRevA.80.013401.

[65] M V Frolov, N L Manakov, T S Sarantseva, and Anthony F Starace. Analytic formulae for high harmonic generation. Journal of Physics B: Atomic, Molecular and Optical Physics, 42(3):035601, jan 2009. doi: 10.1088/0953-4075/42/3/035601. URL https://doi.org/10.1088%2F0953-4075%2F42%2F3%2F035601.

[66] C D Lin, Anh-Thu Le, Zhangjin Chen, Toru Morishita, and Robert Lucchese. Strong-field rescattering physics—self-imaging of a molecule by its own electrons. Journal of Physics B: Atomic, Molecular and Optical Physics, 43(12):122001, jun 2010. doi: 10.1088/0953-4075/43/12/122001. URL https://doi.org/10.1088%2F0953-4075%2F43%2F12%2F122001.

[67] Fran çois Mauger, Paul M. Abanador, Kenneth Lopata, Kenneth J. Schafer, and Mette B. Gaarde. Semiclassical-wave-function perspective on high-harmonic generation. Phys. Rev. A, 93:043815, Apr 2016. doi: 10.1103/PhysRevA.93.043815. URL https://link.aps.org/doi/10.1103/PhysRevA.93.043815.

[68] S. B. Schoun, A. Camper, P. Salières, R. R. Lucchese, P. Agostini, and L. F. DiMauro. Precise access to the molecular-frame complex recombination dipole through high-harmonic spectroscopy. Phys. Rev. Lett., 118:033201, Jan 2017. doi: 10.1103/PhysRevLett.118.033201. URL https://link.aps.org/doi/10.1103/PhysRevLett.118.033201.

[69] G. Doumy, J. Wheeler, C. Roedig, R. Chirla, P. Agostini, and L. F. DiMauro. Attosecond synchronization of high-order harmonics from midinfrared drivers. Phys. Rev. Lett., 102:093002, Mar 2009. doi: 10.1103/PhysRevLett.102.093002. URL https://link.aps.org/doi/10.1103/PhysRevLett.102.093002.

[70] Y. Mairesse, A. de Bohan, L. J. Frasinski, H. Merdji, L. C. Dinu, P. Monchicourt, P. Breger, M. Kovačev, R. Taïeb, B. Carré, H. G. Muller, P. Agostini, and P. Salières. Attosecond synchronization of high-harmonic soft x-rays. Science, 302(5650):1540–1543, 2003. ISSN 0036-8075. doi: 10.1126/science.1090277. URL https://science.sciencemag.org/content/302/5650/1540.

[71] S. Kazamias and Ph. Balcou. Intrinsic chirp of attosecond pulses: Single-atom model versus experiment. Phys. Rev. A, 69:063416, Jun 2004. doi: 10.1103/PhysRevA.69.063416. URL https://link.aps.org/doi/10.1103/PhysRevA.69.063416.

[72] Y. Mairesse, A. de Bohan, L. J. Frasinski, H. Merdji, L. C. Dinu, P. Monchicourt, P. Breger, M. Kovačev, T. Auguste, B. Carré, H. G. Muller, P. Agostini, and P. Salières. Optimization of attosecond pulse generation. Phys. Rev. Lett., 93:163901, Oct 2004. doi: 10.1103/PhysRevLett.93.163901. URL https://link.aps.org/doi/10.1103/PhysRevLett.93.163901.

[73] K. Varjú ‖, Y. Mairesse, B. Carré, M. B. Gaarde, P. Johnsson, S. Kazamias, R. López-Martens, J. Mauritsson, K. J. Schafer, PH. Balcou, A. L'huillier, and P. Salières. Frequency chirp of harmonic and attosecond pulses. Journal of Modern Optics, 52(2-3):379–394, 2005. doi: 10.1080/09500340412331301542. URL https://doi.org/10.1080/09500340412331301542.

[74] Adam Etches, Mette B. Gaarde, and Lars Bojer Madsen. Two-center minima in harmonic spectra from aligned polar molecules. Phys. Rev. A, 84:023418, Aug 2011. doi: 10.1103/PhysRevA.84.023418. URL https://link.aps.org/doi/10.1103/PhysRevA.84.023418.

[75] F. Rosca-Pruna and M. J. J. Vrakking. Experimental observation of revival structures in picosecond laser-induced alignment of I_2. Phys. Rev. Lett., 87:153902, Sep 2001. doi: 10.1103/PhysRevLett.87.153902. URL https://link.aps.org/doi/10.1103/PhysRevLett.87.153902.

[76] P. W. Dooley, I. V. Litvinyuk, Kevin F. Lee, D. M. Rayner, M. Spanner, D. M. Villeneuve, and P. B. Corkum. Direct imaging of rotational wave-packet dynamics of diatomic molecules. Phys. Rev. A, 68:023406, Aug 2003. doi: 10.1103/PhysRevA.68.023406. URL https://link.aps.org/doi/10.1103/PhysRevA.68.023406.

[77] M. C. H. Wong, A.-T. Le, A. F. Alharbi, A. E. Boguslavskiy, R. R. Lucchese, J.-P. Brichta, C. D. Lin, and V. R. Bhardwaj. High harmonic spectroscopy of the cooper minimum in molecules. Phys. Rev. Lett., 110:033006, Jan 2013. doi: 10.1103/PhysRevLett.110.033006. URL https://link.aps.org/doi/10.1103/PhysRevLett.110.033006.

[78] J. Higuet, H. Ruf, N. Thiré, R. Cireasa, E. Constant, E. Cormier, D. Descamps, E. Mével, S. Petit, B. Pons, Y. Mairesse, and B. Fabre. High-order harmonic spectroscopy of the cooper minimum in argon: Experimental and theoretical study. Phys. Rev. A, 83:053401, May 2011. doi: 10.1103/PhysRevA.83.053401. URL https://link.aps.org/doi/10.1103/PhysRevA.83.053401.

[79] S. B. Schoun, R. Chirla, J. Wheeler, C. Roedig, P. Agostini, L. F. DiMauro, K. J. Schafer, and M. B. Gaarde. Attosecond pulse shaping around a cooper minimum. Phys. Rev. Lett., 112:153001, Apr 2014. doi: 10.1103/PhysRevLett.112.153001. URL https://link.aps.org/doi/10.1103/PhysRevLett.112.153001.

[80] Thomas A. Carlson, Manfred O. Krause, and Frederick A. Grimm. Angle resolved photoelectron spectroscopy of cs2 and cos measured as a function of photon energy from 21 to 70 ev. The Journal of Chemical Physics, 77(4):1701–1709, 1982. doi: 10.1063/1.444067. URL https://doi.org/10.1063/1.444067.

[81] Péter Sándor, Adonay Sissay, Fran çois Mauger, Paul M. Abanador, Timothy T. Gorman, Timothy D. Scarborough, Mette B. Gaarde, Kenneth Lopata, Kenneth J. Schafer, and Robert R. Jones. Angle dependence of strong-field single and double ionization of carbonyl sulfide. Phys. Rev. A, 98:043425, Oct 2018. doi: 10.1103/PhysRevA.98.043425. URL https://link.aps.org/doi/10.1103/PhysRevA.98.043425.

[82] M. Bellini, C. Lyngå, A. Tozzi, M. B. Gaarde, T. W. Hänsch, A. L'Huillier, and C.-G. Wahlström. Temporal coherence of ultrashort high-order harmonic pulses. Phys. Rev. Lett., 81:297–300, Jul 1998. doi: 10.1103/PhysRevLett.81.297. URL https://link.aps.org/doi/10.1103/PhysRevLett.81.297.

[83] Mette B Gaarde, Jennifer L Tate, and Kenneth J Schafer. Macroscopic aspects of attosecond pulse generation. Journal of Physics B: Atomic, Molecular and Optical Physics, 41(13):132001, jun 2008. doi: 10.1088/0953-4075/41/13/132001. URL https://doi.org/10.1088%2F0953-4075%2F41%2F13%2F132001.

[84] Cheng Jin, Anh-Thu Le, and C. D. Lin. Medium propagation effects in high-order harmonic generation of ar and n_2. Phys. Rev. A, 83:023411, Feb 2011. doi: 10.1103/PhysRevA.83.023411. URL https://link.aps.org/doi/10.1103/PhysRevA.83.023411.

[85] Olga Smirnova and Misha Ivanov. Multielectron High Harmonic Generation: Simple Man on a Complex Plane, chapter 7, pages 201–256. John Wiley & Sons, Ltd, 2014. ISBN 9783527677689. doi: 10.1002/9783527677689.ch7. URL https://onlinelibrary.wiley.com/doi/abs/10.1002/9783527677689.ch7.

[86] Emmanuel Penka Fowe and Andre D. Bandrauk. Nonlinear time-dependent density-functional-theory study of ionization and harmonic generation in co_2 by ultrashort intense laser pulses: Orientational effects. Phys. Rev. A, 81:023411, Feb 2010. doi: 10.1103/PhysRevA.81.023411. URL https://link.aps.org/doi/10.1103/PhysRevA.81.023411.

[87] Emmanuel Penka Fowe and Andre D. Bandrauk. Nonperturbative time-dependent density-functional theory of ionization and harmonic generation in ocs and cs_2 molecules with ultrashort intense laser pulses: Intensity and orientational effects. Phys. Rev. A, 84:035402, Sep 2011. doi: 10.1103/PhysRevA.84.035402. URL https://link.aps.org/doi/10.1103/PhysRevA.84.035402.

[88] Xi Chu and Gerrit C. Groenenboom. Time-dependent density-functional-theory calculation of high-order-harmonic generation of h_2. Phys. Rev. A, 85:053402, May 2012. doi: 10.1103/PhysRevA.85.053402. URL https://link.aps.org/doi/10.1103/PhysRevA.85.053402.

[89] Daniel Dundas. Multielectron effects in high harmonic generation in n2 and benzene: Simulation using a non-adiabatic quan-

tum molecular dynamics approach for laser-molecule interactions. The Journal of Chemical Physics, 136(19):194303, 2012. doi: 10.1063/1.4718590. URL https://doi.org/10.1063/1.4718590.

[90] Kenneth J. Schafer, Mette B. Gaarde, Arne Heinrich, Jens Biegert, and Ursula Keller. Strong field quantum path control using attosecond pulse trains. Phys. Rev. Lett., 92:023003, Jan 2004. doi: 10.1103/PhysRevLett.92.023003. URL https://link.aps.org/doi/10.1103/PhysRevLett.92.023003.

[91] Jens Biegert, A Heinrichy, Christoph Hauri, W Kornelisy, P Schlupy, M Anscombey, M Gaardez, K Schaferz, and U Kellery. Enhancement of high-order harmonic emission using attosecond pulse trains. Laser Physics, 15:899–902, 02 2005.

[92] Xavier Andrade, Joseba Alberdi-Rodriguez, David A Strubbe, Micael J T Oliveira, Fernando Nogueira, Alberto Castro, Javier Muguerza, Agustin Arruabarrena, Steven G Louie, Alán Aspuru-Guzik, Angel Rubio, and Miguel A L Marques. Time-dependent density-functional theory in massively parallel computer architectures: the octopus project. Journal of Physics: Condensed Matter, 24(23):233202, may 2012. doi: 10.1088/0953-8984/24/23/233202. URL https://doi.org/10.1088%2F0953-8984%2F24%2F23%2F233202.

[93] Xavier Andrade, David Strubbe, Umberto De Giovannini, Ask Hjorth Larsen, Micael J. T. Oliveira, Joseba Alberdi-Rodriguez, Alejandro Varas, Iris Theophilou, Nicole Helbig, Matthieu J. Verstraete, Lorenzo Stella, Fernando Nogueira, Alán Aspuru-Guzik, Alberto Castro, Miguel A. L. Marques, and Angel Rubio. Real-space grids and the octopus code as tools for the development of new simulation approaches for electronic systems. Phys. Chem. Chem. Phys., 17:31371–31396, 2015. doi: 10.1039/C5CP00351B. URL http://dx.doi.org/10.1039/C5CP00351B.

[94] F. Bloch. Bemerkung zur elektronentheorie des ferromagnetismus und der elektrischen leitfähigkeit. Zeitschrift für Physik, 57(7):545–555, Jul 1929. ISSN 0044-3328. doi: 10.1007/BF01340281. URL https://doi.org/10.1007/BF01340281.

[95] P. A. M. Dirac. Note on exchange phenomena in the thomas atom. Mathematical Proceedings of the Cambridge Philosophical Society, 26(3):376–385, 1930. doi: 10.1017/S0305004100016108.

[96] J. P. Perdew and Alex Zunger. Self-interaction correction to density-functional approximations for many-electron systems. Phys. Rev. B, 23:5048–5079, May 1981. doi: 10.1103/PhysRevB.23.5048. URL https://link.aps.org/doi/10.1103/PhysRevB.23.5048.

[97] Miguel A.L. Marques, Micael J.T. Oliveira, and Tobias Burnus. Libxc: A library of exchange and correlation functionals for density functional theory. Computer Physics Communications, 183 (10):2272 – 2281, 2012. ISSN 0010-4655. doi: https://doi.org/10.1016/j.cpc.2012.05.007. URL http://www.sciencedirect.com/science/article/pii/S0010465512001750.

[98] C Legrand, E Suraud, and P-G Reinhard. Comparison of self-interaction-corrections for metal clusters. Journal of Physics B: Atomic, Molecular and Optical Physics, 35(4):1115–1128, feb 2002. doi: 10.1088/0953-4075/35/4/333. URL https://doi.org/10.1088%2F0953-4075%2F35%2F4%2F333.

[99] Johan Mauritsson, Mette B. Gaarde, and Kenneth J. Schafer. Accessing properties of electron wave packets generated by attosecond pulse trains through time-dependent calculations. Phys. Rev. A, 72:013401, Jul 2005. doi: 10.1103/PhysRevA.72.013401. URL https://link.aps.org/doi/10.1103/PhysRevA.72.013401.

[100] Adam Etches and Lars Bojer Madsen. Extending the strong-field approximation of high-order harmonic generation to polar molecules: gating mechanisms and extension of the harmonic cutoff. Journal of Physics B: Atomic, Molecular and Optical Physics, 43(15):155602, jul 2010. doi: 10.1088/0953-4075/43/15/155602. URL https://doi.org/10.1088%2F0953-4075%2F43%2F15%2F155602.

[101] P. M. Kraus, O. I. Tolstikhin, D. Baykusheva, A. Rupenyan, J. Schneider, C. Z. Bisgaard, T. Morishita, F. Jensen, L. B. Madsen, and H. J. Wörner. Observation of laser-induced electronic structure in oriented polyatomic molecules. Nature Communications, 6(1): 7039, 2015. ISSN 2041-1723. doi: 10.1038/ncomms8039. URL https://doi.org/10.1038/ncomms8039.

[102] M. Hentschel, R. Kienberger, Ch Spielmann, G. A. Reider, N. Milosevic, T. Brabec, P. Corkum, U. Heinzmann, M. Drescher, and F. Krausz. Attosecond metrology. Nature, 414(6863):509–513, 2001. ISSN 1476-4687. doi: 10.1038/35107000. URL https://doi.org/10.1038/35107000.

[103] Mette B. Gaarde, Kenneth J. Schafer, Arne Heinrich, Jens Biegert, and Ursula Keller. Large enhancement of macroscopic yield in attosecond pulse train–assisted harmonic generation. Phys. Rev. A, 72:013411, Jul 2005. doi: 10.1103/PhysRevA.72.013411. URL https://link.aps.org/doi/10.1103/PhysRevA.72.013411.

[104] P. Johnsson, R. López-Martens, S. Kazamias, J. Mauritsson, C. Valentin, T. Remetter, K. Varjú, M. B. Gaarde, Y. Mairesse, H. Wabnitz, P. Salières, Ph. Balcou, K. J. Schafer, and A. L'Huillier. Attosecond electron wave packet dynamics in strong laser fields. Phys. Rev. Lett., 95:013001, Jun 2005. doi: 10.1103/PhysRevLett.95.013001. URL https://link.aps.org/doi/10.1103/PhysRevLett.95.013001.

[105] P. Johnsson, J. Mauritsson, T. Remetter, A. L'Huillier, and K. J. Schafer. Attosecond control of ionization by wave-packet interference. Phys. Rev. Lett., 99:233001, Dec 2007. doi: 10.1103/PhysRevLett.99.233001. URL https://link.aps.org/doi/10.1103/PhysRevLett.99.233001.

[106] J. Mauritsson, P. Johnsson, E. Mansten, M. Swoboda, T. Ruchon, A. L'Huillier, and K. J. Schafer. Coherent electron scattering captured by an attosecond quantum stroboscope. Phys. Rev. Lett., 100: 073003, Feb 2008. doi: 10.1103/PhysRevLett.100.073003. URL https://link.aps.org/doi/10.1103/PhysRevLett.100.073003.

[107] Adam Bruner, Samuel Hernandez, François Mauger, Paul M. Abanador, Daniel J. LaMaster, Mette B. Gaarde, Kenneth J. Schafer, and Kenneth Lopata. Attosecond charge migration with tddft: Accurate dynamics from a well-defined initial state. The Journal of Physical Chemistry Letters, 8(17):3991–3996, Sep 2017. doi: 10.1021/acs.jpclett.7b01652. URL https://doi.org/10.1021/acs.jpclett.7b01652.

[108] A. D. Becke and K. E. Edgecombe. A simple measure of electron localization in atomic and molecular systems. The Journal of Chemical Physics, 92(9):5397–5403, 1990. doi: 10.1063/1.458517. URL https://doi.org/10.1063/1.458517.

[109] T. Burnus, M. A. L. Marques, and E. K. U. Gross. Time-dependent electron localization function. Phys. Rev. A, 71:010501, Jan 2005. doi: 10.1103/PhysRevA.71.010501. URL https://link.aps.org/doi/10.1103/PhysRevA.71.010501.

[110] William Ogilvy Kermack and Robert Robinson. Li.—an explanation of the property of induced polarity of atoms and an interpretation of the theory of partial valencies on an electronic basis. J. Chem. Soc., Trans., 121:427–440, 1922. doi: 10.1039/CT9222100427. URL http://dx.doi.org/10.1039/CT9222100427.

[111] Iakov Polyak, Andrew J. Jenkins, Morgane Vacher, Marine E. F. Bouduban, Michael J. Bearpark, and Michael A. Robb. Charge migration engineered by localisation: electron-nuclear dynamics in polyenes and glycine. Molecular Physics, 116(19-20):2474–2489, 2018. doi: 10.1080/00268976.2018.1478136. URL https://doi.org/10.1080/00268976.2018.1478136.

[112] Péter Sándor, Adonay Sissay, François Mauger, Mark W. Gordon, T. T. Gorman, T. D. Scarborough, Mette B. Gaarde, Kenneth Lopata, K. J. Schafer, and R. R. Jones. Angle-dependent strong-field ionization of halomethanes. The Journal of Chemical Physics, 151(19): 194308, 2019. doi: 10.1063/1.5121711. URL https://doi.org/10.1063/1.5121711.

[113] V. Despré, A. Marciniak, V. Loriot, M. C. E. Galbraith, A. Rouzée, M. J. J. Vrakking, F. Lépine, and A. I. Kuleff. Attosecond hole migration in benzene molecules surviving nuclear motion. The Journal of Physical Chemistry Letters, 6(3):426–431, 2015. doi: 10.1021/jz502493j. URL https://doi.org/10.1021/jz502493j. PMID: 26261959.

Graphical Abstract

Multidimensional molecular high-harmonic spectroscopy: a road map for charge migration studies

Daniel R. Tuthill,François Mauger,Timothy D. Scarborough,Robert R. Jones,Mette B. Gaarde,Kenneth Lopata,Kenneth J. Schafer,Louis F. DiMauro

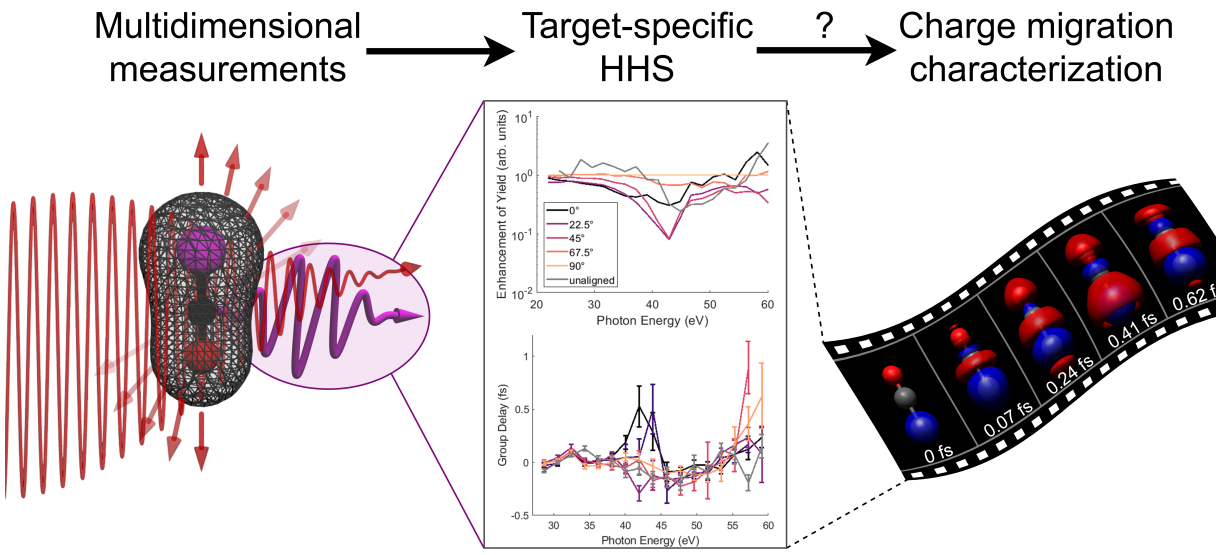

Highlights

Multidimensional molecular high-harmonic spectroscopy: a road map for charge migration studies

Daniel R. Tuthill,François Mauger,Timothy D. Scarborough,Robert R. Jones,Mette B. Gaarde,Kenneth Lopata,Kenneth J. Schafer,Louis F. DiMauro

- High-harmonic spectroscopic measurements of CO_2, CH_3Cl, and OCS
- Extraction of molecular-target-specific information from high-harmonic radiation
- Multidimensional analyses for resolution of convoluted molecular features
- Theoretical short trajectory selection using an attosecond pulse train seed
- Perspectives on extension of high-harmonic spectroscopy to charge migration studies